Available online at www.CivileJournal.org

Civil Engineering Journal

(E-ISSN: 2476-3055; ISSN: 2676-6957)

Vol. 11, No. 11, November, 2025

Predicting the UCS of Industrial Byproduct-Based CLSM Using Machine Learning and Experiments

Chandan K. Singh [1], Divesh R. Kumar [2], K. Lini Dev [1], Warit Wipulanusat [2*]

[1] *Department of Civil Engineering, National Institute of Technology Patna, Patna, 800005, India.*

[2] *Research Unit in Data Science and Digital Transformation, Department of Civil Engineering, Faculty of Engineering, Thammasat School of Engineering, Thammasat University, Pathumthani, Thailand.*

Received 29 May 2025; Revised 19 October 2025; Accepted 25 October 2025; Published 01 November 2025

Abstract

This study investigated the development of sustainable Controlled Low Strength Material (CLSM) using industrial by-products pond ash, fly ash, and red mud as alternatives to conventional concrete constituents. This research employs a dual methodology: comprehensive experimental testing aligned with ASTM standards and the implementation of advanced machine learning (ML) techniques to predict the unconfined compressive strength (UCS) of CLSM mixes. Experimental datasets, generated through the variation of key material and mix design parameters, were utilized to train ensemble-based supervised ML models, including ADAboost, XGBoost, gradient boosting machine (GBM), and random forest (RF). A comparative performance evaluation was conducted, and the XGBoost model emerged as the most accurate predictor, achieving R^2 values of 0.969 for training and 0.933 for testing, surpassing GBM, ADAboost, and RF across multiple performance indicators. The optimal model was subsequently embedded into a graphical user interface (GUI) for UCS prediction. A sensitivity analysis based on the XGBoost model revealed that cement, water, and curing age were the most influential parameters affecting UCS, with cement exhibiting the highest impact value of 0.86 and a relative contribution of 19%. These findings emphasize the significance of these variables in strength development and mix optimization. The integration of experimental validation with predictive modeling not only advances the understanding of CLSM behavior but also underscores the utility of ML in the formulation of sustainable construction materials. This research supports the beneficial reuse of industrial waste, aligns with environmental sustainability goals, and provides an efficient and reliable tool for CLSM mix design.

Keywords: Controlled Low-Strength Material; Pond Ash; Red Mud; Unit Weight; Unconfined Compressive Strength.

1. Introduction

The development of the global economy has largely been driven by industrial progress, which has propelled nations forward through innovation, increased productivity, and employment generation [1, 2]. The rise of factories, large-scale manufacturing, and technological advancements during periods of rapid industrialization has significantly improved living standards and reshaped global economic landscapes [3]. However, alongside these positive contributions, industrial growth has also introduced substantial environmental challenges, particularly in the domain of waste management. As industrial activity has expanded, the volume and complexity of waste generated have increased, posing critical risks to both the environment and public health. Industrial waste often contains hazardous substances, including toxic chemicals and heavy metals, which, if not properly managed, can lead to severe ecological degradation and adverse health effects [4, 5]. In the context of India, industrial byproducts such as pond ash, fly ash, and red mud represent a

* Corresponding author: wwarit@engr.tu.ac.th

http://dx.doi.org/10.28991/CEJ-2025-011-11-04

significant concern. These materials occupy vast tracts of land for disposal and storage, thereby not only consuming valuable space but also contributing to soil, water, and air contamination in surrounding areas [6–8]. Addressing these challenges requires innovative strategies focused on the sustainable reuse of industrial waste, transforming environmental liabilities into valuable construction resources.

One potential solution to reduce the emergence of global waste, such as pond ash, fly ash and red mud, and associated risk is effectively utilizing cementitious material as a fine aggregate or filler for construction purposes. It can also preserve the earth's resources for future generations [9, 10]. Due to the low quality of its ingredients, CLSM can effectively utilize large quantities of industrial byproducts simultaneously for construction purposes [9, 11]. Researchers previously employed industrial waste with appropriate cementitious characteristics to replace the binder, whereas a lower cementitious value byproduct was used as a fine aggregate in the CLSM mix. Controlled low-strength material (CLSM), commonly known as flowable fill, is a self-compacting cementitious material that is primarily used for backfilling and other building applications and requires low uniaxial compressive strength [12]. CLSM is primarily composed of soil, water, cement, fly ash, and fine aggregate, as per ACI 229 [13]. In their study, the unconfined compressive strength (UCS) value ranged between 0.7 and 8.3 MPa, depending on the application. The importance of CLSM may be related to its increased utilization worldwide, since it is the most commonly used approach to recycle industrial byproducts [11]. CLSM has gained widespread use in construction projects worldwide because of its favorable engineering and practical properties. Its ease of placement, flowability, self-leveling, and self-compacting behavior make it a preferred alternative to conventional backfill and other construction materials [14].

In addition, CLSM offers adequate strength and long-term durability, which further enhances its suitability for diverse applications. Among these characteristics, compressive strength is generally regarded as the most critical parameter since it directly influences the structural performance, service life, and overall safety of concrete elements [13]. For this reason, compressive strength testing is routinely carried out, not only to guide the mix design process but also to provide an effective quality control measure during field implementation. The application of machine learning (ML) in predicting the UCS of CLSM, also referred to as flowable fill, has attracted increasing interest because of the diverse and practical uses of CLSM in several engineering applications [6]. Because of their high flowability and self-compacting properties, CLSMs are frequently used as backfill materials behind retaining walls to reduce lateral earth pressures and in the filling of abandoned mines to increase ground stability and prevent subsidence [6]. These materials are also widely applied as bedding layers for pipelines and in pavement sublayers to improve the load distribution, minimize the risk of differential settlement, and streamline construction processes [15, 16]. Various researchers have employed ML techniques to predict the slump, compressive strength, and elastic modulus of plastic concrete mixes incorporating bentonite and sepiolite, demonstrating the potential of these tools in evaluating concrete performance [17, 18]. With the increasing demand for sustainable and efficient construction materials, ML-based prediction of CLSM properties such as UCS represents a promising approach for optimizing mix design and improving structural performance.

In recent years, the rapid advancement of artificial intelligence (AI) has opened new opportunities in the field of construction materials research. In particular, ML algorithms have been increasingly applied to predict various mechanical properties of concrete with high accuracy. These data-driven approaches are capable of identifying complex patterns and relationships within experimental datasets, offering a reliable alternative to traditional empirical or analytical methods [19]. Several studies have applied machine learning models to predict key properties of construction materials. Zhao et al. [20] used support vector regression with optimization techniques to estimate the flowability and UCS of CLSM mixes. As confirmed by experimental assessments, quantitative requirements, and SHAP studies, GA-SVR can predict flowability and UCS with greater accuracy, offering a trustworthy direction for CLSM property prediction. Arachchilage et al. [21] employed ensemble (GBR, RF) and individual (SVR, ANN) machine learning approaches to predict the UCS of alkali-activated slag (AAS)-based cemented paste backfill. Ensemble models outperform individual models, with GBR achieving the highest accuracy. The curing time and water-to-binder ratio were identified as the most influential factors. To forecast the UCS of solid waste–cement-stabilized cohesive soil (SW-CCS), Yao et al. [22] created a database of 474 samples from the literature. After eight artificial intelligence models were tested, the TPE-XGB model was found to have the best precision.

Wang et al. [23] investigated the uniaxial compressive strength (UCS) of a novel coal gangue–hypersaline mine water backfill and employed five soft computing models (DT, RF, GBDT, extra trees, and LightGBM) to predict its UCS. The results show that GBDT yielded the highest accuracy (R^2 = 0.968/0.953), with LightGBM and RF close behind, confirming its strong UCS prediction potential. Using 624 UCS experimental test data, Sun et al. [24] employed the XGBoost algorithm along with five optimizing techniques, such as the WOA, PSO, SSA, GWO and FOA, to predict the UCS of LGF (curing agent)-stabilized marine soft soil (MSS) during dry–wet cycles. Additionally, to maximize the strength, fly ash, lime, and GGBS were mixed together with the MSS. The SSA-XGBoost model (R^2 = 0.9786) proved highly effective for predicting strength in marine projects, surpassing existing techniques.

More recently, gradient boosting models, particularly XGBoost and GBM, have gained popularity for various engineering applications [25–27], including compressive strength prediction of concrete with silica fume and fly ash [28], liquefaction analysis [29, 30], and ground surface settlement prediction [31]. For example, Xiao et al. [32] analyzed CLSM materials without any cement content made of waste glass powder or hydrated lime. Tran et al. [33] employed

the XGBoost model to assess the uplift capacity of 3D rectangular anchors in clay soil. Additionally, some researchers have explored ML models for the estimation of the UCS of soil, consolidation settlement prediction, compressive strength prediction, swelling index prediction, pile bearing capacity prediction, bearing capacity of foundations, and several geotechnical problems [34–36]. ML techniques provide powerful tools for estimating a wide range of material parameters with varying levels of efficiency. These methods have shown strong potential in forecasting compressive strength with high accuracy, offering more reliable predictions than conventional approaches do. In the case of flowable fill materials such as CLSM, accurate assessment of mixture quality is particularly important, as it directly influences performance, durability, and suitability for field applications.

The compressive strength of flowable fill is recognized as one of its most critical mechanical properties and serves as a key indicator of material quality. This parameter plays a central role in determining the performance, durability, and structural reliability of flowable fill in construction applications. However, the application of ensembled ML models, namely, ADAboost, XGBoost, GBM and RF, to estimate the UCS of CLSM mixes containing pond ash, fly ash and red mud remains underexplored. Although ML algorithms function similarly to traditional algorithms, they are more accurate because they can more accurately represent nonlinear behavior than linear behavior. This study explores the use of pond ash, fly ash, and red mud-based CLSM as a sustainable alternative to conventional concrete. This study aims to develop accurate predictive models for the UCS of CLSM using machine learning techniques. Experimental data were generated on the basis of factors influencing UCS and used to train and evaluate models, including ADAboost, XGBoost, GBM, and RF. A comparative analysis identified the most effective model, which was then integrated into a user-friendly graphical user interface (GUI) for practical UCS prediction. This paper details the materials, experimental methods, machine learning frameworks, data preparation, model evaluation, and prediction process.

The significance and novelty of this research are twofold: (1) the execution of experimental work on industrial byproduct-based CLSM following the ASTM standards and (2) the development of predictive models for CLSM compressive strength using advanced ML algorithms. This dual approach not only reinforces the scientific rigor of the experimental phase but also introduces computational efficiency through data-driven modeling. This study specifically focuses on the prediction and comparison of CLSM compressive strength using ensemble-based supervised ML algorithms, including ADAboost, XGBoost, GBM, and RF.

The experimental component is significant in that it establishes standardized testing protocols for CLSM incorporating pond ash, fly ash, and red mud, offering a sustainable substitute for traditional construction materials while addressing the urgent need for effective industrial waste utilization. This aligns with global sustainability goals by mitigating the environmental hazards associated with the large-scale disposal of industrial byproducts. The novelty of this study lies in the application of ensemble ML techniques for predictive UCS modeling for CLSM mixes. These models are trained and validated using experimental datasets to evaluate their accuracy in forecasting compressive strength outcomes. The performance comparison of the developed model reveals the most effective model and provides insights into parameter influence through sensitivity analysis. This integration of experimental validation with machine learning enables accurate strength prediction, reduces reliance on resource-intensive laboratory testing, and facilitates efficient CLSM mix design. As such, this research contributes a novel methodological framework to civil engineering materials science by demonstrating the practical utility of ML in sustainable construction practices.

2. Experimental Program

An experimental program was conducted to collect adequate data for refinement and analysis using several ensembled machine learning boosting models.

2.1. Materials

Initially, this research employed industrial byproducts, specifically pond ash and ordinary Portland cement (OPC) 53 grade, as fine aggregates and binders, respectively, for the preparation of CLSM mixes. In subsequent phases, fly ash, red mud, and locally available sand were introduced as partial replacements for pond ash in the formulation of additional CLSM mixtures, with the aim of evaluating their combined effects on material performance. The pond ash and fly ash used in this study were collected from the dumping site of NTPC Barh, which is located in Bihar, India. Red mud was obtained from HINDALCO Industries, Muri, Jharkhand, which operates a dry disposal system, ensuring material consistency and suitability for construction-related research. To determine the chemical composition of the industrial byproducts, X-ray fluorescence (XRF) at the National Centre for Earth Science Studies (NCESS) in Trivandrum was used. This analysis provided detailed insights into the elemental makeup of the materials, which is essential for understanding their suitability and behavior in construction applications. The detailed elemental compositions of fly ash, red mud, and pond ash are presented in Table 1, providing critical insights into their suitability as sustainable components in CLSM production. The chemical composition data in Table 1 reveal that Fly Ash and Pond Ash are predominantly composed of silica (SiO_2) and alumina (Al_2O_3), indicating their pozzolanic nature. Red mud, while lower in SiO_2, is rich in TiO_2 and Fe_2O_3, reflecting its origin as a byproduct of bauxite refining. In contrast, ordinary Portland cement (OPC) contains significantly more CaO (61.85%), which is essential for cement hydration, but comparatively lower amounts of SiO_2 and Al_2O_3. The high iron and sodium contents of red mud distinguish it chemically from other materials, potentially influencing its suitability for cementitious applications.

Table 1. Chemical composition of the material (wt%)

	Fly Ash	Pond Ash	Red Mud	OPC
SiO_2	54.51	56.6	10.71	20.07
TiO_2	1.91	1.96	16.81	-
Al_2O_3	32.51	30.91	19.91	5.32
MnO	0.04	0.03	0.03	-
Fe_2O_3	4.16	4.22	31.91	4.62
CaO	2.55	1.11	1.74	61.85
MgO	0.52	0.63	0.11	0.83
Na_2O	0.1	0.12	10.21	
K_2O	1.62	1.61	0.07	
P_2O_5	0.57	0.51	0.38	
SO_3	0.25	0.06	0.22	
LOI	0.98	1.95	7.17	

The physical properties presented in Table 2 highlight distinct differences in texture, compaction behavior, and gradation among pond ash, fly ash, and red mud. The grain size analysis indicated that pond ash has a relatively high proportion of fine sand (58.99%) and silt (39.28%), making it a well-graded material with a relatively wide range of particle sizes, as also evidenced by its relatively high uniformity coefficient (Cu = 6.92) and moderate coefficient of curvature (Cc = 0.8), suggesting a relatively stable granular structure. In contrast, fly ash has a higher silt content (77.22%) and significantly lower percentages of sand fractions, which, along with its lower D10, D30, and D60 values, indicates a finer and more poorly graded material, reflected by its lower Cu and Cc values. Red mud has a relatively coarse distribution with notably medium sand content (9.81%) and substantial silt content (64.21%) but lacks uniformity data, making the gradation assessment incomplete. The specific gravity is highest for Red Mud (3.08) because of its high iron content, whereas Fly Ash and Pond Ash are lower and similar (2.04 and 2.03, respectively). The results show that pond ash requires a higher optimum moisture content (OMC) of 38.25% and achieves a lower maximum dry density (MDD) of 9.89 kN/m³, indicating higher porosity (38.42%) and lower compaction efficiency than those of fly ash. These gradation and compaction characteristics are visually supported in Figure 1 through the grain size distribution curve, where Pond Ash exhibits a smoother, more gradual slope indicative of well-graded material, Fly Ash shows a steep curve reflecting finer, uniform particles, and Red Mud displays a distribution curve with a coarser initial segment, suggesting larger particles followed by a finer tail. This gradation behavior directly influences their engineering applications, especially in construction and soil stabilization.

Table 2. Physical characteristics of pond ash, fly ash, and red mud

Property	Pond ash	Fly ash	Red mud
Grain Size Analysis			
Coarse sand size (4.75-2.0 mm)	0.05%	0.18%	0.21%
Medium sand size (2.0-0.425 mm)	1.68%	0.93%	9.81%
Fine sand size (0.425-0.075 mm)	58.99%	20.76%	13.76%
Silt (0.075-.002 mm)	39.28%	77.22%	64.21%
D_{10} mm	0.021	0.011	
D_{30} mm	0.049	0.019	0.007
D_{60} mm	0.14	0.048	0.049
Uniformity coefficient (C_u)	6.92	4.54	-
Coefficient of curvature (C_c)	0.8	0.72	-
Color	Gray	Gray	Red
Specific gravity	2.03	2.04	3.08
Bulk density (kN/m^3)	12.25	15.05	
Proctor compaction test			
OMC (%)	38.25	24.75	
MDD (kN/m^3)	9.89	12.48	
Porosity (%)	38.42	23.81	

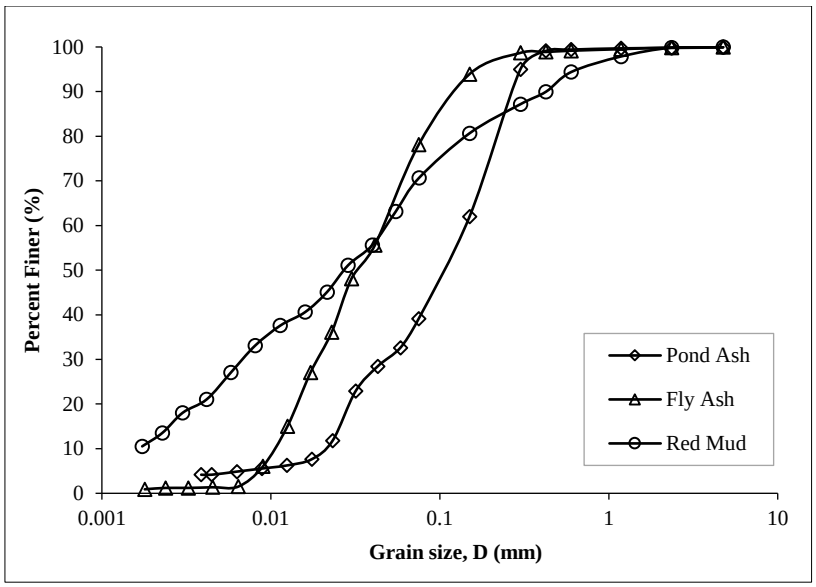

Figure 1. Distribution curve of particle sizes showing grain gradation

2.2. Preparation of Samples and Mixing Method

The performance of the CLSM mix is significantly influenced by the industrial waste incorporated in it [37]. Its strength and ease of flow are two key considerations in its application. The proper ratio of cement to water was determined through trial and error to achieve the required strength of 0.7 MPa and flowability of 295 ± 5 mm for all the CLSM mixes. Cement was applied to the pond ash in this investigation at weight percentages of 3%, 4%, 5%, 6%, and 7%. For the remaining CLSM mixes, pond ash was partially replaced with fly ash (25% & 50%), red mud (25% & 50%), fly ash and red mud (25% & 25%) and sand (25%) with cement contents of 3% and 7% respectively for each mix respectively. To achieve consistent mixing, 1 kilogram of industrial waste was first combined with 3% cement and blended dry for 10 minutes. After ten more minutes, tap water was gradually added, and the mixture was thoroughly mixed. The mix's flowability was monitored continuously while water was gradually added to achieve the desired maximum consistency. Preparation of the CLSM samples was performed following the guidelines specified in ASTM D4832 (2016) [38], ensuring standardized procedures and reliable results.

2.3. Testing Method

To investigate the properties of pond ash-based CLSM, a series of tests were conducted on both fresh and hardened samples. For the assessment of the material in its plastic state, flowability and unit weight measurements were carried out to evaluate workability and consistency. The flowability test was carried out using an open-ended cylindrical mold with dimensions of 75 mm in diameter and 150 mm in height, as shown in Figure 2-a. The procedure followed the standard guidelines provided in ASTM D6103-04 (2004) to ensure the consistency and reliability of the results [39]. These tests provided essential insights into the handling characteristics of the CLSM mixture and ensured that the material met the required standards for placement and compaction. The unit weight of each CLSM mixture was determined in compliance with the ASTM D6023-07 (2007) standard test method, ensuring accurate and consistent measurements across all mixes [40].

(a) (b)

Figure 2. (a) Flowability measurement (b) Sample sealed with cling film and desiccator-cured

The hardened properties of the CLSM mixtures were evaluated by conducting UCS tests, which provided a measure of their load-bearing capacity and overall mechanical performance. All CLSM mixes were made from industrial by-products such as pond ash, fly ash, red mud, and sand, aiming for a target strength of 0.7 MPa with a fixed flowability of 300 mm. Flowability was checked before preparing the UCS samples. Each sample was cast in molds with a diameter of 38 mm and a height of 76 mm. The samples were cured at 30°C with 100% humidity prior to testing. After preparation, the samples were carefully wrapped in cling film to prevent moisture loss and then stored in a standard desiccator, as illustrated in Figure 2-b. UCS tests were performed on three samples from each mixture after 7, 14, 28, 56, and 90 days, and a UCS test for the pond ash-based CLSM mixture was also performed for a 268-day curing period following ASTM D4832 (2016) [38]. Scanning electron microscopy (SEM) was employed to investigate the surface features and microstructural details of the materials at high magnifications. For this study, SEM observations were conducted on the raw industrial by-products, namely, pond ash and red mud, as well as on CLSM samples incorporating 7% ordinary Portland cement (OPC) after a 28-day curing period.

The primary objective of the SEM test was to investigate the microstructural changes that occur during the hydration and hardening processes, providing insight into the development of strength and bonding within the cementitious matrix. SEM was performed via a Carl–Zeiss Sigma microscope at the research laboratory of NIT Durgapur. The SEM results are presented in Figure 3-a Pond ash, Figure 3-b Red mud, and Figure 4-a Pond ash-based CLSM and Figure 4-b Pond ash and red mud-based CLSM mixtures. Before imaging, the samples were oven-dried to remove any moisture, finely ground to ensure a representative surface, and then coated with a thin layer of gold. This gold coating enhances the conductivity of the sample, preventing charging under the electron beam and ensuring clearer, more accurate imaging. Scanning electron microscopy (SEM) analysis provided detailed insights into the microstructural characteristics of the material. The obtained micrographs revealed the development of various hydration products, such as calcium silicate hydrate (C–S–H), ettringite, and needle-like or flaky crystalline structures, which contributed to the mechanical strength and durability of the CLSM. By comparing the microstructures of the raw materials and cured CLSM, the extent of the pozzolanic reactions and bonding between the particles could be evaluated. These microscopic insights help to validate the mechanical test results (such as unconfined compressive strength) by correlating them with the internal structure, porosity, and distribution of reaction products, thereby offering a comprehensive understanding of material performance.

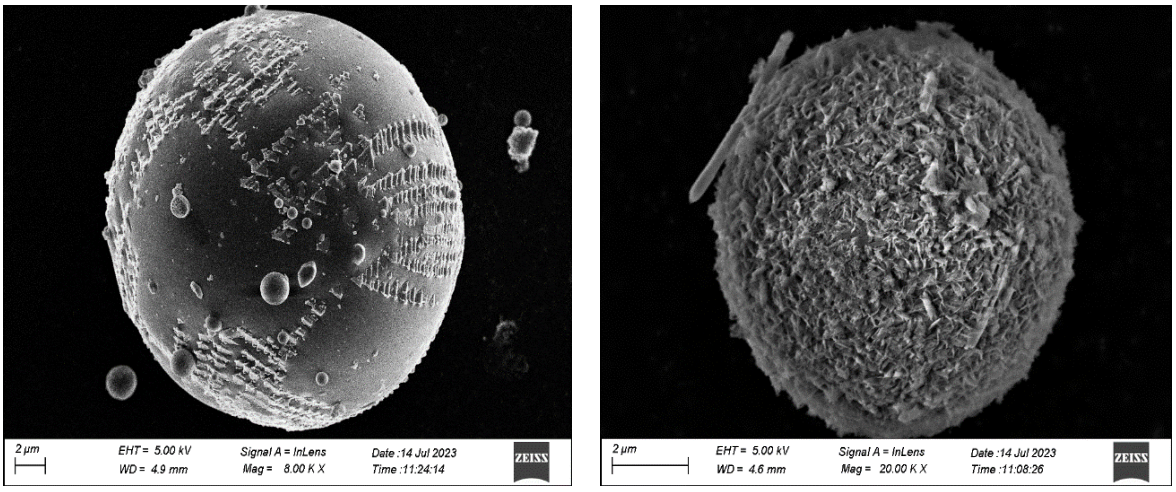

(a) Pond ash (b) Red mud

Figure 3. SEM analysis of (a) Pond ash, and (b) Red mud

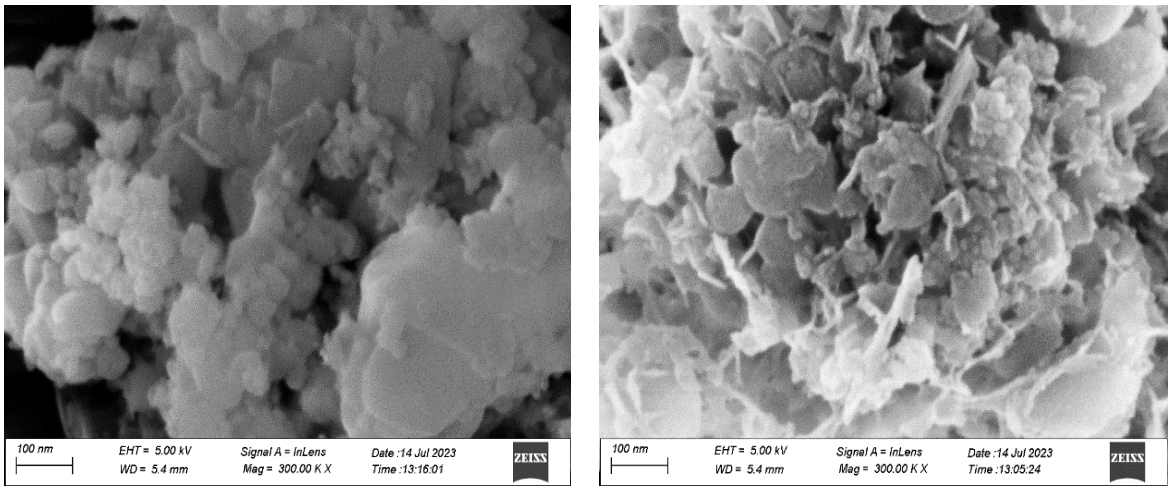

(a) Pond ash-based CLSM with 7% cement content (b) Pond ash and red mud-based CLSM with 7% cement content

Figure 4. SEM analysis of (a) Pond ash-based CLSM and (b) Pond ash and red mud-based CLSM Mixtures

2.4. Mix Proportion

The CLSM mixes used for testing and evaluation include C3PA, C4PA, C5PA, C6PA, and C7PA, which are basically pond ash (PA)-based CLSM mixes with 3%, 4%, 5%, 6% and 7% cement content (C) by weight of total waste incorporated. The total weight of the incorporated industrial waste was fixed at 1 kg for each CLSM mix. C3PAFA0.25, C3PAFA0.5, C7PAFA0.25, and C7PAFA0.5 represent pond ash- and fly ash (FA)-based CLSM mix with 3% and 7% cement content, respectively. Fly ash was used as a partial replacement for pond ash, varying from 25% to 50%. C3PARm0.25, C3PARm0.5, C7PARm0.25, and C7PARm0.5 represent pond ash- and red mud (Rm)-based CLSM mix with 3% and 7% cement content, respectively. Red mud was also used as a partial replacement for pond ash, varying from 25% to 50%. C7PAFA0.25Rm0.25 and C7PAFA0.5Rm0.25 represent pond ash- and red mud (Rm)-based CLSM mix with a 7% cement content. Here, fly ash and red mud are used as partial replacements of pond ash, varying from 25% to 50%. Additionally, C7PAS and C7FAS are basically pond ash (PA)- and sand (S)- and fly ash (FA)- and sand (S)-based CLSM mixes with a 7% cement content for each mixture.

3. Properties of Materials

3.1. Descriptive Statistics of the Datasets

Table 3 presents the descriptive statistics of the study variables, offering an overview of how the different materials used in preparing the CLSM mixtures vary and contribute to their overall characteristics. The independent variables include cement, pond ash, fly ash, red mud, sand, water, and curing age, whereas compressive strength is the primary output or dependent variable. The cement content ranges from 30 gm to 80 gm, reflecting different mix designs aimed at exploring the role of cement in the final strength of the CLSM mix. Pond ash, an industrial by-product, ranges from 0 g to 1000 g, indicating its substantial inclusion for assessing its sustainability and effect on material properties. The amount of fly ash used ranges from 0 gm to 750 gm, further emphasizing the use of by-products as a partial replacement for cement. Red mud, which is another industrial by-product, varies from 0 gm to 500 gm, and the sand content ranges from 0 gm to 250 gm, with both materials acting as fillers in the mix. Water, crucial for hydration and workability, is used in amounts ranging from 556 gm to 795 gm. The curing age, a significant factor in the strength development of CLSM mix, varies widely from 7 days to 268 days. The output variable, compressive strength, ranges from 0.07 MPa to 2.14 MPa, reflecting the combined effect of the input materials and curing time on the material's mechanical properties. This wide range of input values and compressive strengths illustrates the comprehensive approach used to evaluate various mix proportions and the role of the byproducts used to prepare the CLSM mix.

Table 3. Detailed descriptive statistics of the experimental dataset

Index	Cement (gm)	Pond Ash (gm)	Fly Ash (gm)	Red Mud (gm)	Sand (gm)	Water (ml)	Age (Day)	UCS (MPa)
Minimum	30	0	0	0	0	556	7	0.07
Maximum	80	1000	750	500	250	795	268	2.14
Mean	55.24	678.57	166.67	135.71	19.05	663.67	56.13	0.62
Standard Error	1.70	25.92	22.61	17.91	6.50	8.09	6.25	0.05
Median	60	750	0	0	0	640	28	0.45
Kurtosis	-1.44	-0.21	-0.36	-0.48	8.67	-1.21	4.26	0.03
Skewness	-0.40	-0.48	1.01	0.96	3.24	0.50	2.11	0.95

The frequency histograms, combined with kernel density estimate (KDE) curves, for all the features considered in this study, i.e., cement, pond ash, fly ash, red mud, sand, water, age, and UCS, offer a clear visualization of their distributions in the dataset. Figure 5 shows the frequency histogram with the KDE distribution for all the variables. For the cement content, which ranges from 30 gm to 80 gm, the histogram and KDE curve reveal how often different quantities are used, potentially indicating a concentration around moderate amounts. Pond ash, with a wide range from 0 gm to 1000 gm, has a distribution that may reflect frequent usage of larger amounts, and the KDE curve smooths out this frequency, highlighting the most likely values. Similarly, the histogram for fly ash content (0 gm to 750 gm) depicts its usage pattern, with the KDE indicating whether lower amounts are more common. For red mud (0 gm to 500 gm), the histogram shows how often each amount is present in the mix, with the KDE curve providing a smooth distribution of the data to reveal frequent quantities. Sand, ranging from 0 gm to 250 gm, has a peak distribution at approximately 0 gm, few samples have a sand content of 250 gm, and the KDE illustrates the most likely sand amounts used in the study. The water content, ranging from 556 g to 795 g, is a critical variable for workability, and the KDE curve highlights whether certain water quantities dominate the dataset. The curing age, ranging from 7 days to 268 days, has a histogram that shows how frequently different curing times are applied, with the KDE smoothing out this variation to reveal common curing periods, potentially emphasizing the predominance of shorter or longer durations. Finally, the UCS, which ranges from 0.07 MPa to 2.14 MPa, is the primary output variable, and its histogram and KDE curve reflect how often different strength values are achieved, possibly skewing toward lower strengths at early ages and higher strengths for more optimized mixes. This combination of frequency histograms and KDE curves provides a comprehensive understanding of the distributions and likelihoods of various input values and their impacts on compressive strength, revealing key trends in the dataset utilized in this study.

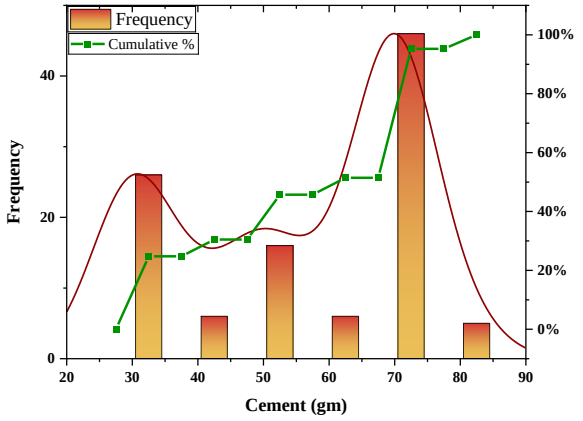

(a) Cement

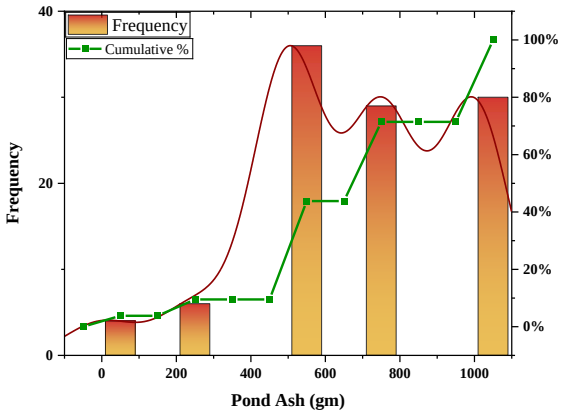

(b) Pond ash

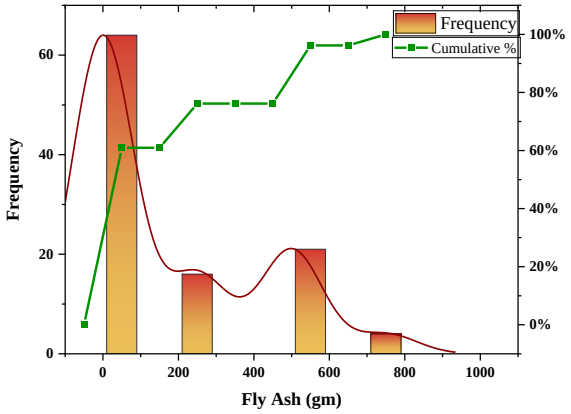

(c) Fly ash

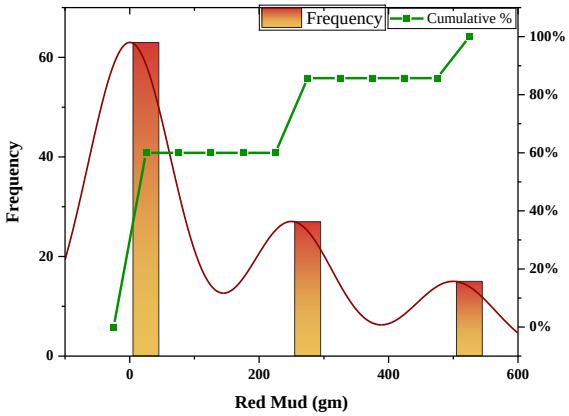

(d) Red mud

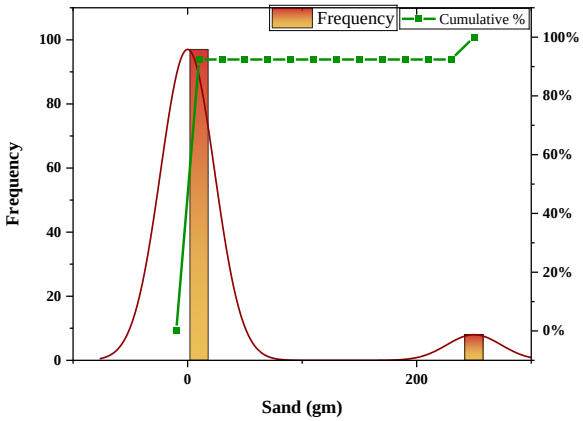

(e) Sand

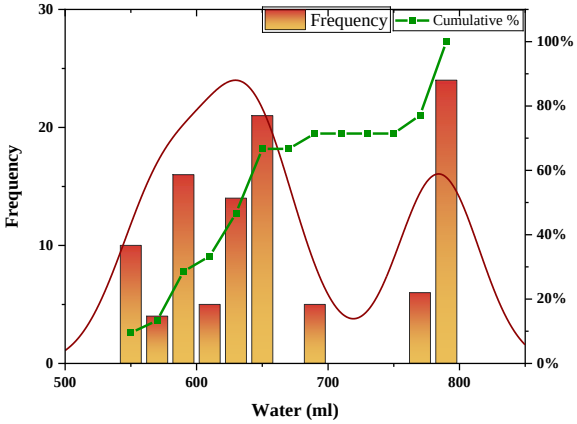

(f) Water

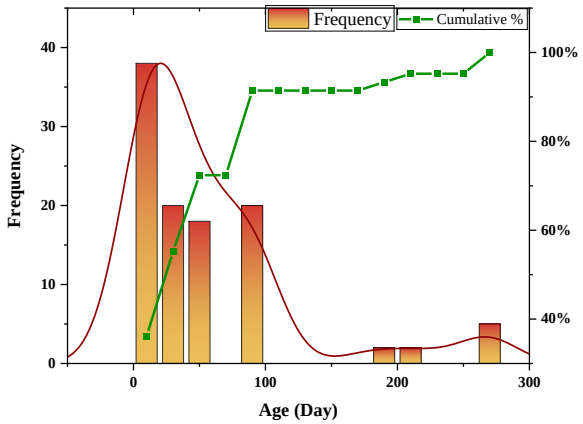

(g) Age

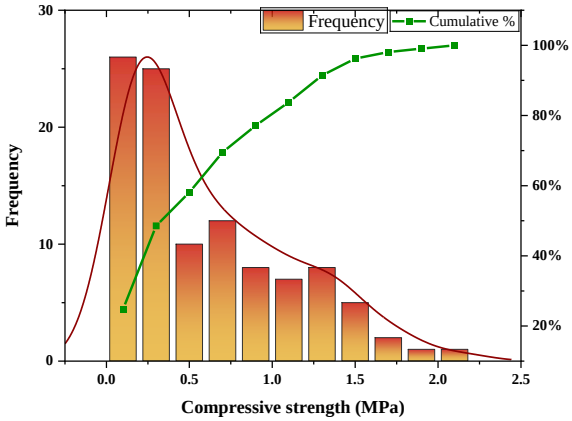

(h) Compressive strength

Figure 5. Frequency histogram with KDE distribution for variables

Figure 6 shows the correlation heatmap for the study conducted in the present work. A Pearson correlation heatmap visually represents the strength and direction of the linear relationship between variables through the intensity of color. In this particular case, the variables include cement, pond ash, fly ash, red mud, sand, water, curing age, and UCS. The heatmap uses color-coded circles to indicate the correlation coefficients, where a red circle represents the highest positive correlation of +1, a blue circle indicates the strongest negative correlation of −1, and a white circle represents no correlation (0). The Pearson correlation heatmaps for the variables cement, pond ash, fly ash, red mud, sand, water, curing age, and UCS reveal key relationships. The UCS shows a moderate positive correlation with the cement content (+0.61), indicating that an increase in the cement content enhances the compressive strength. In contrast, pond ash has a moderate negative correlation with UCS (−0.44), suggesting that a higher pond ash content reduces UCS. Fly ash and UCS are weakly positively correlated (+0.17), whereas red mud is positively correlated (+0.38), indicating that these materials slightly contribute to increased compressive strength. The sand content shows a weak correlation with UCS (+0.12), indicating minimal impact, and the water content shows a weak negative correlation (−0.22), implying that excess water slightly reduces the UCS. Additionally, the UCS has a moderate positive correlation with the curing age (+0.42), reflecting the strength gain over time due to continued hydration. Water also strongly correlates with other materials. There is a strong positive correlation between water and pond ash (+0.86), indicating that a relatively high pond ash content increases the water demand. Conversely, water and fly ash have a moderate negative correlation (−0.68), suggesting that increasing fly ash reduces the amount of water needed, likely because fly ash has a positive impact on mix workability. These correlations help understand the interactions between the materials and how they collectively influence the compressive strength of the mixture.

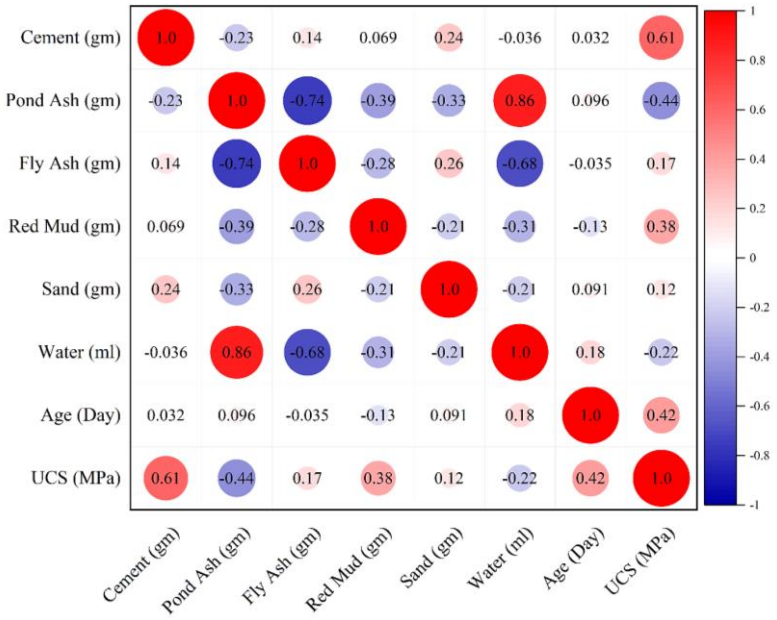

Figure 6. Correlation heatmap chart

3.2. Data Preparation and Modeling

In the data preprocessing step, data normalization is performed, which is crucial for optimizing the learning rate and enhancing the predictive accuracy of the ML algorithms. Data normalization transforms the original dataset into a unitless format, ensuring that all the input features and output values are on the same scale. This is particularly crucial when the data consists of parameters with varying units, magnitudes, and ranges, as it eliminates any discrepancies between numerical ranges, thereby preventing certain features from disproportionately influencing the model. The learning capability of the proposed machine learning algorithms, trained by training datasets, is affected by the scale of the input data during the learning process. Large variations between features can cause models to converge slowly or to become stuck in local minima during training, as certain features dominate the learning process because of their larger numerical values. Therefore, it is necessary to rescale the data to a common scale; in this study, all the variables were normalized between 0 and 1 [41–45]. In this study, the entire dataset of both input and output variables was normalized using specific mathematical equations, namely, Equations 1 and 2. These equations transform the raw data into a range of [0, 1], effectively removing units and making the data suitable for training the proposed models

$$Input_{normalized,i} = \frac{Input_{actual,i} - Input_{min,i}}{Input_{max,i} - Input_{min,i}} \quad (1)$$

$$Output_{normalized,i} = \frac{Output_{actual,i} - Output_{min,i}}{Output_{max,i} - Output_{min,i}} \quad (2)$$

Normalizing the dataset allows learning algorithms to interpret the data more consistently, resulting in faster convergence and higher prediction accuracy. Normalization also reduces the risk of overfitting by ensuring that no larger-scale characteristic dominates the model's learning process. Normalizing the data using Equations 1 and 2 is crucial for ensuring that machine learning models can effectively interpret both the input features and output targets, resulting in more trustworthy predictions. This preprocessing procedure not only improves model performance but also ensures that the model is generalizable to previously unseen data. In this study, a total of 105 CLSM mix samples were prepared and tested by varying the proportions of cement, pond ash, fly ash, red mud, and sand. All the measurements were obtained from controlled laboratory experiments. Prior to model development, all the features were normalized to ensure uniform scaling. After all the features are normalized, the complete dataset is randomly divided into two sets: a training set and a testing set. To train the machine learning models, the complete dataset was split randomly into training and testing sets at an 80–20 ratio, which is a broadly typical exercise in machine learning model training. The training set consists of 84 data points that are used for model construction, and the remaining 21 datasets are utilized for testing the developed models.

3.3. Model Evaluation Indicators

To assess the effectiveness of the proposed models, six performance metrics were employed and analyzed in detail. The coefficient of determination (R^2) was used as a primary indicator, which measures the correlation between the experimental and model-predicted UCS values. R^2 values approaching 1 signify a stronger model fit. In addition, the adjusted coefficient of determination ($AdjR^2$) was calculated to assess the developed models, making it a more reliable measure of goodness of fit for experimental and predicted UCS values and providing a more accurate measure when multiple variables are involved. The Nash–Sutcliffe efficiency (NS) was also used to evaluate the predictive ability of the models relative to the observed mean, whereas the variance accounting factor (VAF) provided insight into the percentage of variance explained by the predictions. The performance index (PI) further quantifies model accuracy by combining different aspects of prediction quality. Finally, several error metrics, including the weighted mean absolute percentage error (WMAPE), root mean square error (RMSE), and mean absolute error (MAE), were applied to quantify deviations between the predicted and observed values. Together, these metrics offer a comprehensive evaluation of model performance from multiple perspectives, ensuring a robust and reliable assessment [30, 46–49]. The ideal values of the performance parameters are presented in Table 4. The mathematical expressions of the performance and error metrics are presented in Equations 3 and 8.

$$R^2 = \frac{\sum_{i=1}^{n}(d_i - d_{avg})^2 - \sum_{i=1}^{n}(d_i - y_i)^2}{\sum_{i=1}^{n}(d_i - d_{avg})^2} \quad (3)$$

$$VAF = \left(1 - \frac{var(d_i - y_i)}{var(d_i)}\right) \times 100 \quad (4)$$

$$NS = 1 - \frac{\sum_{i=1}^{n}(d_i - y_i)^2}{\sum_{i=1}^{n}(d_i - d_{avg})^2} \quad (5)$$

$$WMAPE = \frac{\sum_{i=1}^{n}\left|\frac{d_i - y_i}{d_i}\right| \times d_i}{\sum_{i=1}^{n} d_i} \quad (6)$$

$$RMSE = \sqrt{\frac{1}{n}\sum_{i=1}^{n}(d_i - y_i)^2} \quad (7)$$

$$MAE = \frac{1}{n}\sum_{i=1}^{n}|(y_i - d_i)| \quad (8)$$

where; d_i and d_{avg} denote the experimental UCS value and its average UCS value, respectively, and y_i denotes the model-predicted UCS value.

Table 4. Ideal value of performance metrics

Metrics	R^2	VAF	NS	WMAPE	RMSE	MAE
Ideal value	1	100	1	0	0	0

4. Methodology and Theoretical Background

4.1. Details of Machine Learning Models

4.1.1. Gradient Boosting Machine (GBM)

Boosting methods are essentially based on sequential ensembles of weak learner models that are marginally better than random models. Gradient boosting is a regression technique that is similar to boosting [50]. GBM algorithms are designed to generate an estimate $G(x)$ of an unknown target function $G^*(x)$ on the basis of a given training dataset

$\{x_i, y_i\}_1^N$, where each input instance x_i corresponds to an output value y_i. The primary objective of the GBM is to find a function $G(x)$ that minimizes the expected value of a specified loss function, denoted as $\phi(y, G(x))$, thereby improving the accuracy of predictions. In the gradient boosting framework, this estimation is achieved iteratively by constructing a weighted sum of simpler base functions, which collectively serve as an approximation of $G^*(x)$. This approach allows the model to progressively reduce prediction errors, as illustrated in Equation 9.

$$G_i(x) = G_{i-1}(x) + \rho_i h_i(x) \tag{9}$$

where; ρ_i is the ith function $h_i(x)$ weight in this case. The estimate is constructed iteratively. A constant approximation of $G^*(x)$ is first derived as shown in Equation 10.

$$G_0(x) = arg\min_{\alpha} \sum_{i=1}^{N} \phi(y_i, \alpha) \tag{10}$$

Subsequent models must be developed in the direction of the minimal value using Equation 11.

$$(\rho_m, h_m(x)) = \arg\min_{\rho,h} \sum_{i=1}^{N} \phi(y_i, G_{i-1}(x_i) + \rho h(x_i)) \tag{11}$$

Each h_m may be considered a greedy step in gradient descent optimization for G^* rather than a straightforward solution to the optimization problem. Each model "h_m" is trained on a fresh dataset $D = \{x_i, r_{mi}\}_{i=1}^N$, with the residuals r_{mi} being found using the Equation 12.

$$r_{mi} = \left[\frac{\partial \phi(y_i, G(x))}{\partial G(x)}\right]_{G(x)=G_{i-1}(x)} \tag{12}$$

Next, a line search optimization problem is solved to obtain the value of ρ_m.

The procedure terminates early if the residuals for some loss functions are fully fitted by the model h_m, in which case the error is minimized in the subsequent iteration. Many hyperparameters are set to control the gradient boosting additive process. A reasonable method to regularize gradient boosting $G_i(x) = G_{i-1}(x) + v\rho_i h_i(x)$ with $v = (0.1)$, often regarded as 0.1, is to minimize the gradient decent of each step. Moreover, greater regularization may be attained by simplifying the learned models. In the case of decision trees, we may set a restriction on the count of occurrences needed to split a node or the depth of the tree. Some gradient boosting variants use hyperparameters to randomize base learners, such as random subsampling without replacement, which can improve the ensemble's generalizability [50]. According to Natekin & Knoll (2013) [51], the gradient boosting technique is a highly proficient regression method capable of managing intricate nonlinear function relationships.

4.1.2. Adaptive Boosting (ADAboost)

One of the most potent machine learning techniques is the ADAboost approach, which Freund first presented [52]. To create a stronger number of models, this approach is initially constructed on the simplest classifiers. This approach may be used to address regression and classification challenges, similar to the tree approach. It creates a model that is less vulnerable to overfitting and more accurate by taking into account the weights of each learner. The algorithm steps are summarized below. Find the least skilled learner's regression error percentage. Determine the largest possible error using Equation 13.

$$E_t = \max|y_i - h_t(x_i)|, i = 1,2, \dots\dots, N \tag{13}$$

where; x_i and y_i indicate the input data; N is the number of samples; and $h_t(x)$ represents the weak learner of the t-th iteration.

By using the regression loss function, the relative error for all of the samples can be calculated via Equation 14.

$$\epsilon_{ti} = \frac{|y_i - h_t(x_i)|}{E_t} \tag{14}$$

Calculate the rate of regression error using Equation 15;

$$\epsilon_t = \sum_{i=1}^{h} w_{ti}\, \epsilon_{ti} \tag{15}$$

where in the above expression, the term w_{ti} represents the weight of sample x_i.

1) Find the least skilled learner's weight coefficient (α) using Equation 16.

$$\alpha = \frac{\epsilon_t}{1-\epsilon_t} \tag{16}$$

2) Updated sample weights for the t+1 iteration cycle via Equations 17 and 18.

$$W_{t+1}(x_i) = \frac{W_t(x_i)}{Z_t} \alpha_t^{1-\epsilon_{ti}} \quad (17)$$

$Z_t = \sum_{i=1}^{N} W(x_{ti})\, \alpha_t^{1-\epsilon_{ti}}$; Z_t is the normalization factor (18)

3) The highly skilled learner is created via Equation 19.

$H(x) = \sum_{t=1}^{T} w_{ti} \ln\left(\frac{1}{\alpha_t}\right) f(x)$. $f(x)$ is the median value of $\alpha_t h_t(x)$ (t = 1, 2, …, T) (19)

Furthermore, the AdaBoost technique simply needs minor parameter modifications, including the regression loss function, iteration count and decision tree depth. As a result, it has been widely applied in many other sectors.

4.1.3. XGBoost

Recently, Chen & Guestrin [53] developed the machine learning algorithm known as XGBoost, which is currently in extensive use across a range of applications. It may be used for a wide range of applications because of its organization, portability, versatility, and quickest and most integrated decision tree algorithm. The algorithm integrates the cause-based decision tree (CBDT) and gradient boosting machine (GBM) into a single effective method. It expands the tree boosting approach's ability to process nearly all data types quickly and consistently. XGBoost is a versatile and strong tool that can handle user-defined goal functions for the intended output in addition to a broad variety of classifications and regressions. Processing large datasets with many characteristics and classifications is another use of XGBoost. Additionally, this approach offers feasible and competent solutions for novel optimization issues, especially when accuracy and efficiency trade-offs are considered.

XGBoost's objective function has a striking resemblance to those of previous machine learning models; this similarity might be attributed to the integration of its regular term and loss function. The regular term controls the model's complexity, whereas the loss function controls the model's accuracy. XGBoost improves the output of the loss function by calibrating the previous prediction at each iteration using the residual. Regularization is incorporated into the goal function by XGBoost to reduce the risk of overfitting during the calibration stage using Equation 20.

$$L(\phi) = l(\phi) + \Omega(\phi) = \sum_{i=1}^{n} l(y_i, \hat{y}_i) + \sum_{K=1}^{K} \Omega(f_k) \quad (20)$$

The decision tree (DT) regularization term was proposed by Chen & Guestrin (2016) [53] as follows in Equation 21:

$$\Omega(f) = yT + \frac{1}{2}\lambda \sum_{j-1}^{T} \omega_j^2 \quad (21)$$

Here, Φ denotes the parameters learned from training data, Ω is the regularization component, l is the training loss, y_i is the observed value, T is the number of leaves, λ is the penalty weight, and ω_j is the score of the j-th leaf.

The tree ensemble model introduces functions as parameters (Equation 22), where the prediction for the i^{th} instance at the t^{th} iteration is updated using a new function $f(x_i)$:

$$L^{(t)} = \sum_{i=1}^{n} l(y_i, \hat{y}_i^{t-1} + f_t(x_i) + \Omega(f_t) \quad (22)$$

This objective is approximated using a second-order Taylor expansion [53, 54], leading to Equation 23:

$$L^{(t)} \approx \sum_{i=1}^{n} \left[g_i \omega_{q(x_i)} + \frac{1}{2}(h_i \omega_{q(x_i)}^2 \right] + \gamma T + \frac{1}{2}\lambda \sum_{j=1}^{T} \omega_j^2 \quad (23)$$

where g_i and h_i are the first and second derivatives of the loss function, respectively, and where $q(x_i)$ maps instance i to its corresponding leaf. Aggregating over each leaf node yields Equation 24:

$$L^{(t)} \approx \gamma T + \sum_{j=1}^{t} \left[\sum_{i \in i_j} (g_i)\, \omega_j + \frac{1}{2}\left(\sum_{j=1} h_i + \lambda\right) \omega_j^2 \right] \quad (24)$$

where; $G_j = \sum_{i \in i_j} g_i$ and $H_j = \sum_{i \in i_j} h_i$ are defined as where I_j represents the set of samples in leaf j. Minimizing a quadratic function allows the optimization of the objective function, which quantifies the change in model output resulting from a node split in the decision tree. A split is retained only if it improves model performance; otherwise, it is discarded. Regularization is applied to help prevent overfitting [55].

4.1.4. Random Forest (RF)

The random forest (RF) model is widely used in decision tree learning to carry out regression and classification. Breiman [56] introduced the RF model framework. The model creates a classifier with strong simplification capabilities by combining the results of each individual decision tree using a particular combination strategy. There are two methods used to perceive RF randomness: (1) Not all features are employed in the training process; instead, the characteristics utilized in training are selected at random when each decision tree is constructed. (2) The bootstrap samples are randomly selected from the training data to train the model. Because the development process for each decision tree is distinct, productivity may be increased during the model generation phase by using parallel processing. The process for creating a model involves three main steps. Step 1: Feature selection: Out of all M features available as input variables, m features are randomly selected for each DT to prevent overfitting. In the second step, each decision tree is constructed using bootstrap sampling, where n samples are drawn with replacement from the full dataset of size N, whereas the remaining samples, known as out-of-bag (OOB) data, are reserved for evaluating model performance. In the final step, after all n decision trees have been trained, the prediction error for each tree is calculated using its corresponding OOB data, and the overall model output is obtained by averaging the predictions of all individual trees. To ensure optimal performance, several hyperparameters must be defined in advance, including the total number of trees, the maximum number of features considered at each split, the minimum number of samples required at a leaf node, the minimum number of samples needed to split an internal node, the maximum depth of each tree, and the maximum number of leaf nodes. For a detailed discussion of the RF model's ultimate decision outcome, see Belgiu & Drăgu [57] and Breiman [56].

5. Results and Discussion

5.1. Unconfined Compressive Strength

Controlled low-strength material (CLSM) mixes incorporating industrial byproducts such as fly ash, pond ash, and red mud exhibit variable compressive strengths depending on the mix design and material properties. Owing to its pozzolanic activity, fly ash enhances long-term strength development in CLSM, often achieving compressive strengths in the range of 1–8 MPa, making it suitable for non-structural applications such as backfilling and trench filling. Pond ash, with its coarser particles, contributes to improved workability and moderate strength, typically in the lower range of CLSM applications (0.7-3 MPa). Red mud, owing to its high alkalinity and iron oxide content, can act as a stabilizing agent, but its inclusion must be optimized to avoid excessive setting times or durability issues. Blending these byproducts with cement or lime can further increase the strength while providing an eco-friendly solution for waste utilization. Figures 7 to 9 illustrate the variation in UCS over different curing periods for all the CLSM mixes. Among the mixes, C7PA (7% cement) exhibited the highest strength, reaching approximately 1.0 MPa after 90 days, followed by C6PA, C5PA, C4PA, and C3PA in descending order. The rate of strength gain is more rapid in the early curing period (up to ~28 days) and tends to plateau thereafter, indicating progressive pozzolanic reactions between the cement hydration products and pond ash. This pattern demonstrates how stronger pond ash-based combinations become with greater cement doses, demonstrating that cement functions as the main binder and activator in stabilizing pond ash for possible engineering uses [6, 58].

However, the incorporation of fly ash (0.25 and 0.5 replacement levels) modified the strength gain behavior. Mix C7PAFA0.5 has the highest strength, showing a steady increase up to 90 days, whereas the other cement mixes (C3PAFA0.25 and C3PAFA0.5) have reduced strengths. This suggests that fly ash enhances long-term strength when combined with higher cement content, but excessive replacement in low-cement mixes reduces performance [59]. However, the addition of red mud also contributes to strength development. Among the tested mixes, C7PARm0.5 achieves the maximum compressive strength, exceeding 2.0 MPa at 90 days. This trend indicates that a higher cement content coupled with 0.5 red mud replacement improved the pozzolanic activity and strength. In contrast, low-cement mixes (C3PARm0.25 and C3PARm0.5) exhibit limited performance. The data clearly demonstrate a progressive increase in UCS as the curing time increases, indicating that the continued hydration and pozzolanic reactions contribute to strength gain. Notably, the most significant increase in strength occurs within the first 28 days of curing, which is consistent with the typical behavior of cementitious materials, where early-age reactions dominate the strength development process. Beyond 28 days, although the UCS continues to increase, the rate of strength gain diminishes, suggesting that the primary hydration reactions have substantially completed and that the material begins to approach its long-term strength potential. This trend underscores the importance of the early curing phase in achieving the desired mechanical performance of CLSM.

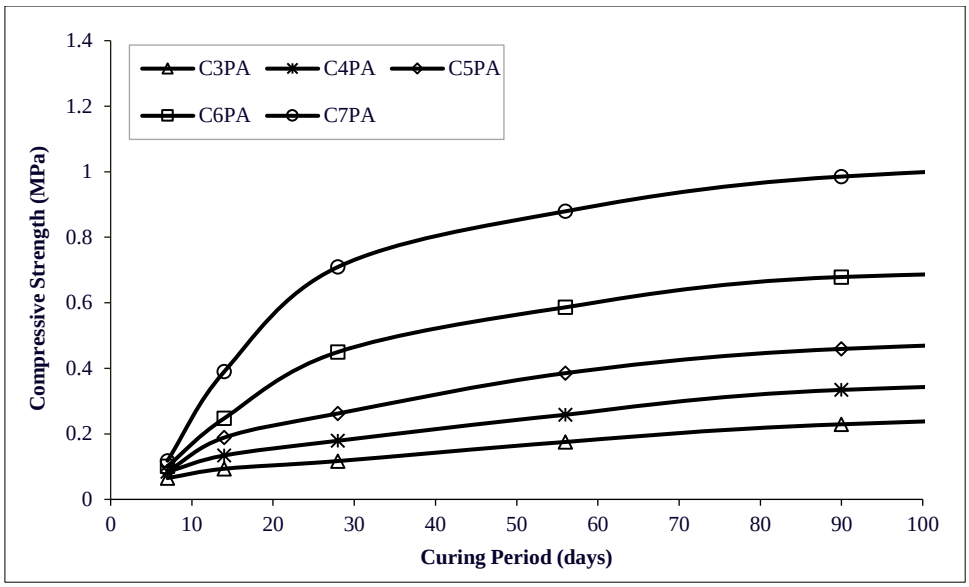

Figure 7. Compressive strength development with curing period of pond ash based CLSM mix

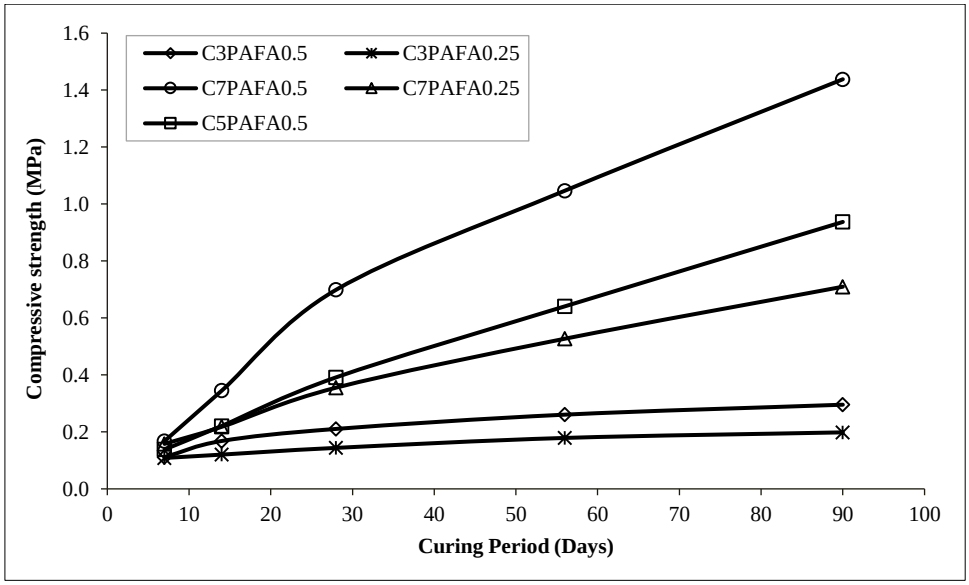

Figure 8. Compressive strength development with curing period of pond ash and fly ash based CLSM mix

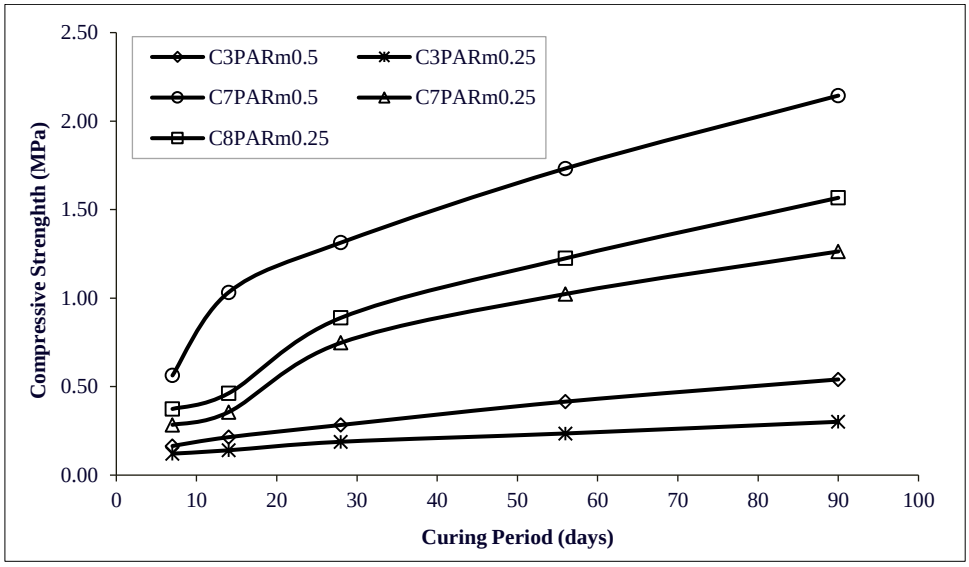

Figure 9. Compressive strength development with curing period of pond ash and red mud based CLSM mix

5.2. Configuration of the Developed Models

In the development of ML models, hyperparameters play a crucial role in guiding the learning process and directly affect the effectiveness of predictive models. For the proposed ML models, the hyperparameters must be defined prior to training begins. Their proper selection can significantly impact model accuracy, convergence speed, and generalization to new data. To optimize the performance of models such as GBM, AdaBoost, XGBoost, and RF, hyperparameter tuning is crucial. Grid search is a systematic approach for hyperparameter tuning that involves defining a set of values for each hyperparameter and then exhaustively searching through the combinations to find the best configuration. In this technique, first, a dictionary of hyperparameters and their respective ranges is created. Next, the "GridSearchCV" library function from "scikit-learn" is used to set up the grid search, which automatically evaluates all possible combinations of these hyperparameters. To optimize key settings such as the number of trees, learning rate, and maximum tree depth, this approach was applied in this study.

To ensure the reliability of the results, 5-fold cross-validation was incorporated into each round of tuning, allowing each hyperparameter combination to be evaluated across multiple data splits rather than relying on a single train–test partition. The model is then trained by fitting the grid search object to the training data, where 5-fold cross-validation is employed to assess model performance for each combination. Afterward, the optimal value of hyperparameters was obtained for the provided training dataset on the basis of the 5-fold cross-validation results, and these tuned values of hyperparameters were utilized to develop models that are used to make predictions on the test data, optimizing their performance. The details of the search range and optimal value obtained for each developed model are summarized in Table 5. The methodology flowchart illustrates the predictive framework for estimating the compressive strength of CLSM mixtures using ensemble modeling techniques, as presented in Figure 10.

Table 5. Details of the grid search range and optimal value for the developed model

Algorithm	Hyperparameters	Search range	Values
XGBoost	N_estimator	[50, 100, 150, 200, 250, 300]	150
	Max_depth	[3, 4, 5, 7]	5
	learning rate	[0.01, 0.1, 0.2, 0.3]	0.1
	Gamma	[0, 0.1, 0.2]	0.1
	subsample	[0.7, 0.8, 0.9, 1]	0.8
AdaBoost	N_estimator	[50, 100, 150, 200, 250, 300]	250
	Max_depth	[1, 3, 4, 5, 7]	5
	learning rate	[0.01, 0.1, 0.2, 0.3]	0.3
	Gamma	[0, 0.1, 0.2]	0.3
RF	N_estimator	[50, 100, 150, 200, 250, 300]	200
	Max_depth	[1, 3, 4, 5, 7]	6
	learning rate	[0.01, 0.1, 0.2, 0.3]	0.1
	Minimum sample leaf	[1, 2, 3, 4]	3
	Max features	[auto, sqrt, log2]	auto
GBM	N_estimator	[50, 100, 150, 200, 250, 300]	150
	Max_depth	[1, 3, 4, 5, 7]	7
	learning rate	[0.01, 0.1, 0.2, 0.3]	0.2
	subsample	[0.7, 0.8, 0.9, 1]	0.7
	Minimum sample leaf	[1, 2, 3, 4]	2

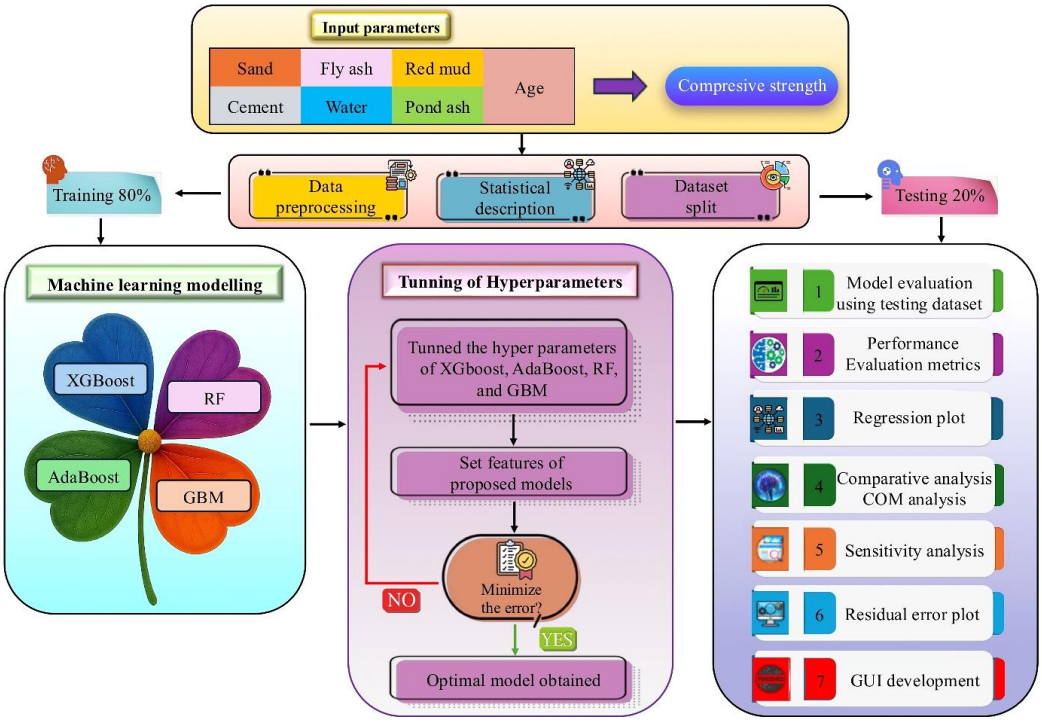

Figure 10. Methodology flowchart

This flowchart provides a comprehensive overview of the sequential steps involved, starting from data collection and preprocessing, followed by feature selection and model training, and culminates in the evaluation and validation of the ensemble models.

5.3. Statistical Details of the Results

Four ML models, namely, GBM, AdaBoost, XGBoost, and random forest, were evaluated, and the accuracy and performance of the developed models were assessed using multiple performance indicators. Key metrics, including R^2, VAF, NS, WMAPE, RMSE, and MAE, were used to measure each model's predictability, error, and efficiency. While all the models performed well on the training data, with R^2 values ranging from 0.948 to 0.969, the testing results showed some divergence, with XGBoost achieving the highest R^2 values of 0.969 in the training phase and 0.933 in the testing phase, indicating strong generalizability to unseen data. However, reliance solely on R^2 is insufficient, as different metrics capture unique aspects of model performance, such as RMSE, WMAPE, NS, VAF, and MAE. As per the results presented in Table 6, the GBM model in the training phase obtained R^2 values of 0.984, 0.966 for AdaBoost, 0.969 for XGBoost, and 0.960 for RF, indicating that all the models exhibit strong predictive capabilities. The test datasets further demonstrate the models' generalizability, with R^2 values of 0.866 for GBM, 0.907 for AdaBoost, 0.933 for XGBoost, and 0.870 for RF. These results show that XGBoost performs the best in terms of both training accuracy and testing accuracy, followed by AdaBoost, RF, and GBM. However, the evaluation goes beyond R^2 values; additional indices such as VAF, NS, WMAPE, RMSE, and MAE were also considered to ensure a holistic assessment. The optimal model should achieve near-ideal values across these metrics, reinforcing the importance of comprehensive evaluation beyond a single metric. Table 6 shows that the combination of all indices provides a clearer picture of model performance, and XGBoost appears to outperform the other models in terms of all the performance metrics, particularly in the testing phase.

Table 6. Performance indices for all proposed models

Performance indices	GBM		AdaBoost		XGBoost		RF	
	Train	Test	Train	Test	Train	Test	Train	Test
R^2	0.948	0.866	0.966	0.907	0.969	0.933	0.960	0.870
WMAPE	0.121	0.245	0.069	0.250	0.093	0.240	0.099	0.271
NS	0.945	0.865	0.964	0.900	0.968	0.889	0.958	0.855
RMSE	0.054	0.093	0.044	0.080	0.041	0.084	0.047	0.096
VAF	94.708	86.625	96.507	90.308	96.830	91.320	95.980	86.066
MAE	0.033	0.059	0.019	0.060	0.025	0.057	0.027	0.065

5.4. Discussion of the Results

Figure 11 shows a comparison of the actual and predicted compressive strengths of all the models evaluated on the training and testing datasets. In the image, the solid yellow line represents the ideal regression line where the predicted values perfectly match the actual values. Each model's individual plots depict the relationship between the predicted compressive strength and the actual experimental values for the training and testing datasets. The regression plots for the proposed models illustrate how closely the predictions align with the actual compressive strength measurements, providing insight into their predictive accuracy. For the XGBoost model, the regression plot demonstrates a strong correlation between the predicted and actual values, indicating its effectiveness in capturing the underlying patterns in the predicted compressive strength value. Similarly, the AdaBoost model closely clusters the predicted values around the y = x line, demonstrating its superior performance in minimizing prediction error. The RF model also displays a relatively good fit, although its performance is marginally less accurate than that of XGBoost and AdaBoost. In contrast, the GBM model, while generally consistent, shows a slightly wider dispersion of points, suggesting some limitations in its predictive capability compared with XGBoost, AdaBoost and RF. Overall, the regression plots reveal that XGBoost and AdaBoost significantly outperform the RF and GBM in terms of predicting the compressive strength of CLSM, highlighting their robustness and effectiveness in handling complex relationships within the dataset.

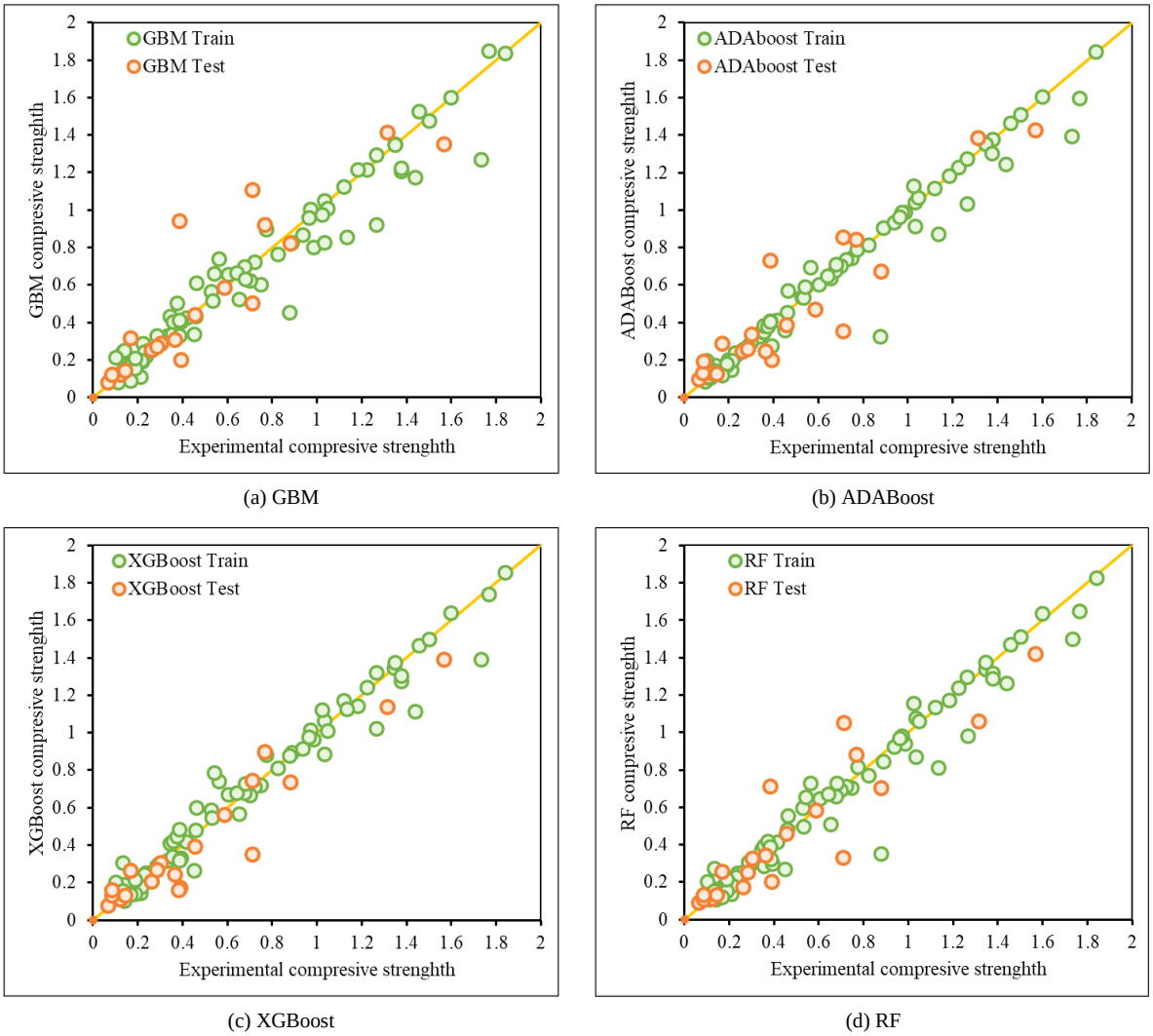

(a) GBM (b) ADABoost

(c) XGBoost (d) RF

Figure 11. Comparision of actual and predicted compresive strength of all models

5.5. Model Ranking Using Comprehensive Measure (COM)

he comprehensive measure (COM) method, as proposed by Kumar et al. [19], is a strategy used to rank machine learning models by combining multiple performance metrics into a single, cohesive score. Relying solely on an individual metric such as R^2, RMSE, or MAPE may not adequately reflect a model's true performance. To address this

limitation, the COM approach was employed in this study to deliver a more balanced and insightful assessment by integrating these metrics into one composite indicator. This method is particularly useful for reconciling conflicting trends among different indicators and offers a clearer comparison of model effectiveness. The COM value is calculated using Equation 25:

$$COM = \left(\frac{1}{3}\frac{RMSE_{Training} \times MAPE_{Training}}{R^2_{Training}}\right) + \left(\frac{2}{3}\frac{RMSE_{Testing} \times MAPE_{Testing}}{R^2_{Testing}}\right) \quad (25)$$

In this formulation, greater weight is assigned to the testing phase (two-thirds) than to the training phase (one-third) to prioritize the model's generalization ability. This weighted approach ensures that the evaluation reflects both accuracy and robustness. A lower COM score corresponds to superior model performance across the selected criteria. Among the models, XGBoost achieved the lowest COM score of 3.013, as shown in Table 7, securing the first rank. It showed the best balance between high accuracy (R^2 = 0.9689 training, 0.9327 testing) and low error metrics, making it the most robust and generalizable model. The random forest algorithm ranked second (COM = 3.565), with strong overall performance but a slightly lower generalization capability than XGBoost, as reflected by the decrease in R^2 and increase in RMSE in the testing phase. The GBM, which was ranked third, demonstrated good performance (COM = 3.792), but higher errors in the MAPE affected its ranking. ADAboost, despite having strong training R^2 (0.9655) and the lowest RMSE, ranked fourth (COM = 4.288). The COM ranking thus highlights XGBoost as the most reliable and accurate model for the given dataset, making it the best choice for predictive modeling of the UCS of CLSM.

Table 7. Results of the comprehensive measure

Model	Training phase			Testing phase			COM	Ranking
	R^2	RMSE	MAPE	R^2	RMSE	MAPE		
GBM	0.9484	0.0544	24.1656	0.8663	0.0930	46.5419	3.792	Third
ADAboost	0.9655	0.0442	11.6323	0.9070	0.0801	69.7909	4.288	Fourth
XGBoost	0.9689	0.0413	21.5519	0.9327	0.0843	44.9223	3.013	First
RF	0.9601	0.0473	19.8333	0.8704	0.0964	46.8506	3.565	Second

5.6. Residual Error Plot

The error residual histograms of the proposed models are presented in Figure 12. Illustrations of error residual histograms offer valuable insights into how well the models perform in predicting the compressive strength of the CLSM mix. The presented histograms represent the distribution of the predicted model error for UCS values, which ideally follow a normal distribution centered around zero. When the residuals are symmetrically distributed around zero with minimal deviation, the model is considered accurate. For the GBM model during the training phase, the mean residual error is 0.022, with a standard deviation (SD) of 0.111. This indicates that the predictions are generally close to the true values, with minor deviations. In the AdaBoost model, the mean error is slightly lower at 0.018, and the SD is 0.090, reflecting a better concentration of errors around the mean, implying a more consistent model. XGBoost, with a near-zero mean (−0.001) and the smallest SD of 0.086, demonstrates the most balanced error distribution during training, indicating its high accuracy. Finally, the RF model has a mean error of 0.018 and an SD of 0.097, positioning it between AdaBoost and GBM in terms of error dispersion.

However, in the case of the testing phase, the residual distributions shift. The GBM model has a negative mean of −0.017 and a larger SD of 0.193, suggesting that it slightly underpredicted on average and that its predictions were more widespread. The AdaBoost model yields a mean error of 0.029, andSD for the predicted error is 0.164, indicating positive bias but retaining moderate prediction consistency. XGBoost's mean of 0.081 and SD of 0.156 suggest an upward bias in its predictions, although the error spread remains relatively contained. RF, with a mean of 0.039 and the highest SD of 0.197, indicates greater error variability in testing, suggesting that while it performs well on training data, it may be more sensitive to unseen data. Overall, XGBoost maintains the tightest error distribution during both the training and testing phases but has a slight upward bias in predictions during testing. GBM and RF show increased error variability during the testing phase, which could point to challenges in generalizing across datasets. AdaBoost shows a balanced performance with moderate deviations and minimal bias across both phases.

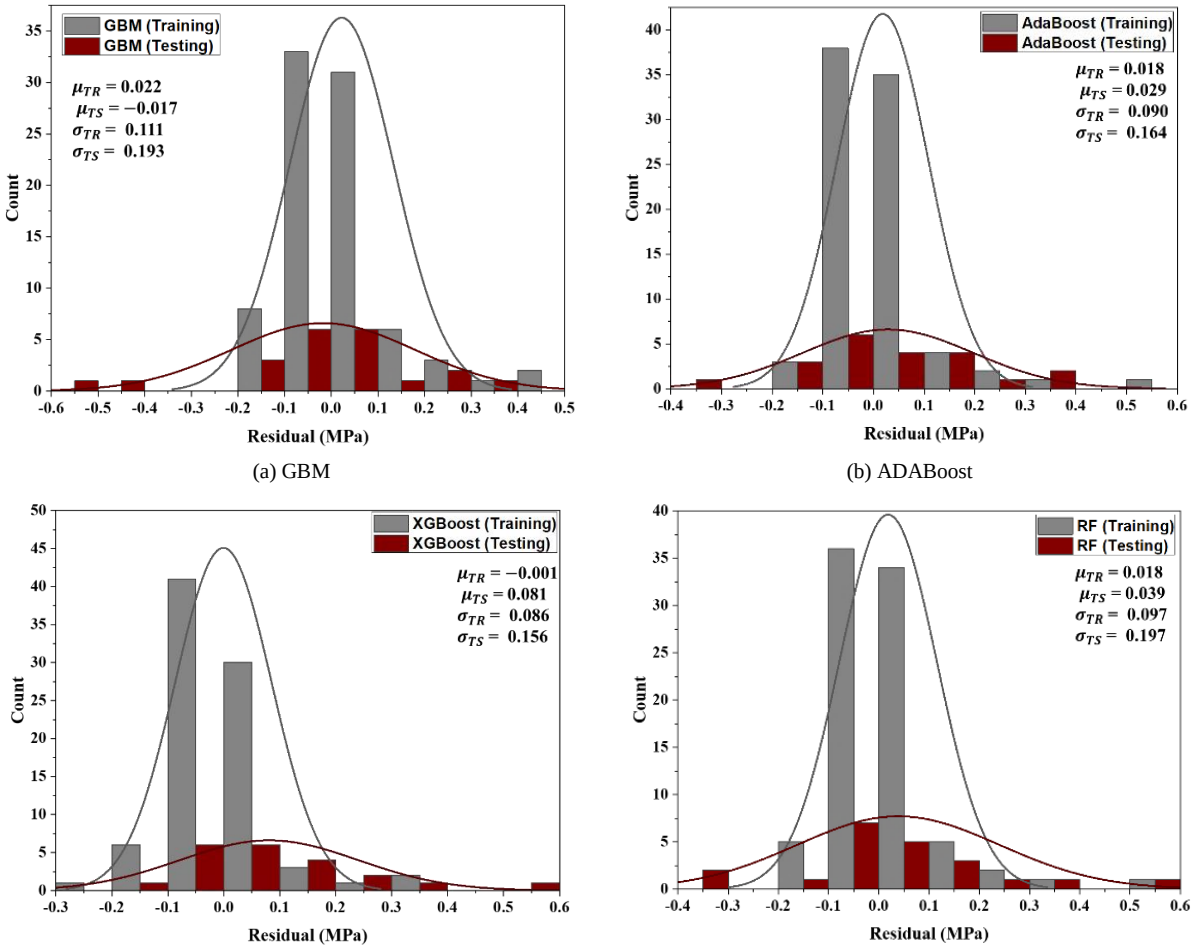

(a) GBM (b) ADABoost

(c) XGBoost (d) RF

Figure 12. Residual error histogram

5.7. Sensitivity Analysis

In the context of predicting the UCS of CLSM mixes, a sensitivity analysis was conducted on the best-performing XGBoost model using cosine amplitude method (CAM) [60]. This analysis aimed to evaluate the influence of various input variables, i.e., cement, pond ash, fly ash, red mud, sand, water, and curing age, on the predicted compressive strength. Sensitivity analysis helps in understanding how changes in the input parameters impact the model output, allowing researchers to focus on the most critical factors affecting the compressive strength of CLSM mixture as shown in Figure 13. Cement was found to have the greatest impact on compressive strength, with an impact value of 0.86, indicating its crucial role in strength development. Water and curing age followed with impact values of 0.76 and 0.71, respectively, underscoring the importance of proper hydration and curing for achieving optimal strength. Red mud, with an impact of 0.65, and pond ash, with an impact of 0.63, also played important roles, suggesting that these industrial byproducts can effectively contribute to the mixture's strength. Fly ash, with an impact value of 0.55, had a moderate influence, primarily enhancing durability rather than significantly affecting strength. Sand had the least impact at 0.29; although it provides bulk and contributes to the overall mixture stability, it does not play a significant role in strength development, primarily serving as a filler material. It has a minimal effect on the compressive strength.

Overall, the analysis highlights that cement, water, and curing age are the most influential factors, whereas industrial byproducts such as pond ash and red mud offer potential for sustainable mix designs without heavily compromising strength. Figure 14 shows the relative significance of each variable's impact on the UCS of the CLSM mix. The results revealed that the cement content was the most influential factor, accounting for 19% of the relative impact on the compressive strength. Water, the second most influential variable at 17%, plays a critical role in hydration and workability; thus, maintaining an appropriate W/C ratio is essential to prevent compromising the integrity of the structure. The curing age also significantly influences the compressive strength, with a relative impact of 16%, emphasizing the necessity of adequate curing durations to promote optimal hydration and pozzolanic reactions. Red mud and pond ash, contributing 15% and 14%, respectively, further highlight the positive effects of these industrial byproducts on the compressive strength of CLSM, likely due to their pozzolanic properties. In contrast, fly ash has a relatively lower impact at 12%, indicating that its role in strength enhancement is less significant than that of other constituents. Finally, sand had the least influence at 7%.

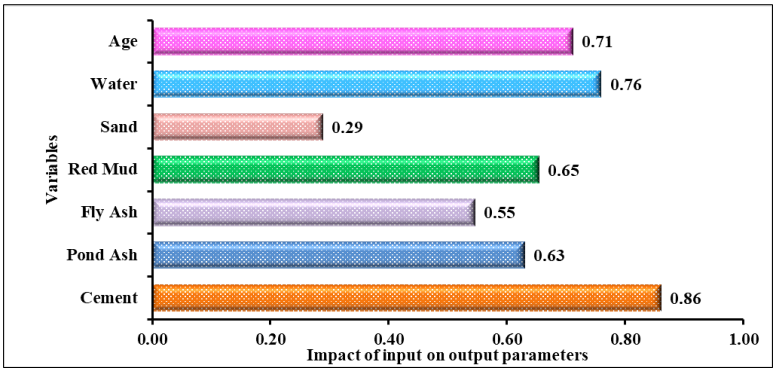

Figure 13. Impact of input parameters on compressive strength

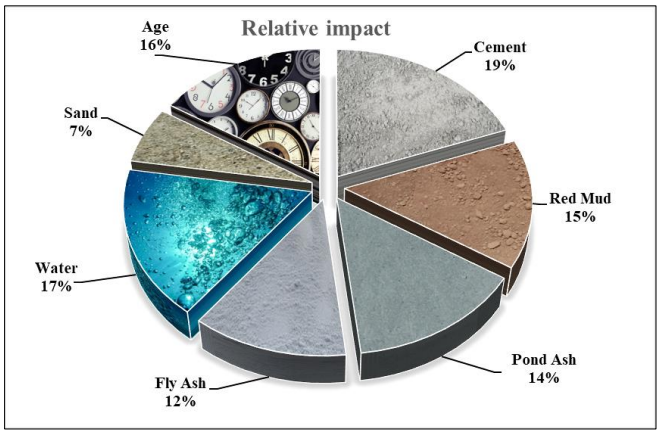

Figure 14. Relative impact of input parameters on compressive strength

5.8. Comparison with Previous Studies

Table 8 summarizes the performance of various models from previous studies alongside those developed in the current research. Across studies, support vector regression (SVR) and several ML models, such as MARS, GBM, and XGBoost, have demonstrated strong predictive capability for CLSM compressive strength, with R^2 values typically ranging from 0.86 to above 0.97. In this study, the XGBoost model achieved training and testing R^2 values of 0.969 and 0.933, respectively, which compare favorably with prior results, highlighting its robustness and accuracy. While some earlier studies reported slightly higher test R^2 values, differences in input variables, dataset size, and source materials likely contributed to these variations. The presented results confirm the suitability of ensemble learning techniques, particularly XGBoost, for reliable UCS prediction in CLSM mixes.

Table 8. Comparison results of previous studies

References	Variables	Models	R^2
Zhao et al. [20]	Sand, Soil, Cement, Fly Ash, Water, SP, CA	SVR-PSO	Train R^2 = 0.931 Test R^2 = 0.972
		SVR-GA	Train R^2 = 0.934 Test R^2 = 0.969
		SVR=GS	Train R^2 = 0.907 Test R^2 = 0.979
Shin et al. [61]	Cement, Fly Ash, Sludge, Fine Aggregate, and Water	Genetic Algorithm	R^2 = 0.864
Dev et al. [45]	Cement, Fines content in the ash, Pond ash, Fly ash, Water, Flowability, Curing period	MARS	Train R^2 = 0.964 Test R^2 = 0.943
		FN	Train R^2 = 0.910 Test R^2 = 0.908
		GMDH	Train R^2 = 0.923 Test R^2 = 0.923
		MPMR	Train R^2 = 0.955 Test R^2 = 0.941

Dev et al. [59]	Cement, Bentonite, Water, Curing period	MARS	Train R^2 = 0.990 Test R^2 = 0.963
		ENN	Train R^2 = 0.733 Test R^2 = 0.726
		XGBoost	Train R^2 = 0.967 Test R^2 = 0.923
		GBM	Train R^2 = 0.955 Test R^2 = 0.920
Current study	Cement, Pond Ash, Fly Ash, Red Mud, Sand, Water, Age	GBM	Train R^2 = 0.948 Test R^2 = 0.866
		ADABoost	Train R^2 = 0.966 Test R^2 = 0.907
		XGBoost	Train R^2 = 0.969 Test R^2 = 0.933
		RF	Train R^2 = 0.960 Test R^2 = 0.870

5.9. Graphical User Interface (GUI)

A graphical user interface (GUI) was developed for the prediction of the UCS of CSLM mixes using a machine learning-based XGBoost regression algorithm using Tkinkter [62]. The model takes seven key input parameters, Cement, Pond Ash, Fly Ash, Red Mud, Sand, Water, and Age, to estimate the UCS (MPa). The GUI interface for predicting the UCS of the CLSM mix is shown in Figure 15. For a particular set of input values, the experimental UCS was found to be 1.376 MPa, whereas the GUI-based prediction yielded a value of 1.378 MPa. The absolute error between the predicted and experimental values is 0.002 MPa, which corresponds to a percentage error of approximately 0.145%. This minimal error demonstrates the high accuracy and reliability of the XGBoost model integrated into the GUI for practical applications in geotechnical and construction material analysis.

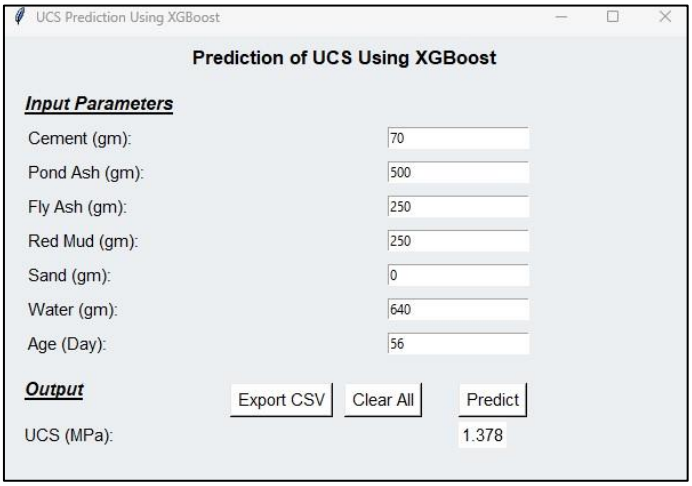

Figure 15. GUI for predicting the compressive strength of the CLSM mix

6. Conclusions

This study demonstrates the successful development of CLSM using industrial byproducts such as pond ash, fly ash, and red mud as sustainable alternatives to conventional materials. For the CLSM mix, all experimental procedures were conducted following ASTM standards, thereby validating the mechanical viability of these materials in CLSM mixtures. ML models, specifically ensemble methods such as GBM, AdaBoost, XGBoost, and RF, were employed to predict the UCS of the mixtures. The major conclusions of the current study are summarized in bullet points as follows:

- The compressive strength of CLSM mixes incorporating fly ash, pond ash, and red mud varies with mix composition and curing duration, with fly ash contributing to long-term strength gains (1–8 MPa), pond ash enhancing workability and moderate strength (0.7–3 MPa), and red mud acting as a stabilizer when properly dosed.
- UCS development is most pronounced within the first 28 days of curing due to early hydration and pozzolanic activity, with strength gain continuing at a slower rate, thereafter, highlighting the critical importance of early-age curing in optimizing CLSM performance.

- The predicted UCS values of the CLSM mixes generated by the proposed ensemble models (GBM, AdaBoost, XGBoost, and RF) closely match the experimental results, with XGBoost demonstrating the highest accuracy, achieving R^2 values of 0.969 in training and 0.933 in testing, outperforming AdaBoost, RF, and GBM across multiple statistical indices, including RMSE, MAE, NS, and VAF, confirming its superior predictive performance and generalizability.
- COM analysis revealed that the XGBoost model is the most accurate and generalizable model (COM = 3.013), outperforms RF, GBM, and AdaBoost, confirming its robustness and reliability for predicting the UCS of CLSM mixes.
- The analysis of the error residual histograms reveals that among the evaluated models, XGBoost results in the most balanced and tightly distributed residuals during both the training and testing phases, with the lowest standard deviation (0.086 in training and 0.156 in testing), indicating high accuracy and consistent performance.
- The developed GUI-based XGBoost model provides a fast, accurate, and user-friendly tool for predicting the UCS of CSLM mixes, achieving a prediction accuracy of 99.85% with an absolute error of only 0.002 MPa compared with the experimental value of 1.376 MPa, making it highly suitable for practical engineering and construction material applications.

This study, while effectively demonstrating the potential of ensemble machine learning models for predicting the UCS of CLSM mixtures incorporating industrial byproducts, is subject to certain limitations. A primary constraint is the relatively small dataset used for model training and evaluation, which may affect the generalizability of the developed models. Moreover, the absence of external validation using independent datasets or field-scale data further limits the robustness and practical applicability of the developed models. To enhance model reliability and applicability across diverse construction environments, future studies should incorporate larger and more heterogeneous datasets, encompassing variations in geographic and material conditions. The model performs well within the tested range of variables, but its accuracy at extreme input values may be limited by fewer data points. Expanding the dataset to include these extremes will improve model robustness in future work.

Additionally, the current investigation primarily addresses short-term UCS prediction without considering other critical performance attributes, such as long-term durability, resistance to freeze–thaw cycles, sulfate attack, or other environmental stressors, that influence CLSM performance in real-world scenarios. Environmental parameters such as ambient temperature, humidity, and in situ compaction conditions, which significantly affect the mechanical behavior and setting characteristics of CLSM, were also excluded from the model input variables.

To strengthen the applicability of machine learning models in construction materials research, future research should integrate a broader spectrum of input variables and performance metrics, incorporate field-scale experimental validations, and evaluate the adaptability of these predictive models under diverse construction and environmental conditions. Such efforts would contribute to the development of more comprehensive, reliable, and practically implementable tools for sustainable construction material design and optimization.

7. Declarations

7.1. Author Contributions

Conceptualization, C.K.S., D.R.K., and K.L.D.; methodology, D.R.K., K.L.D., and W.W.; software, D.R.K.; validation, C.K.S., D.R.K., and W.W.; formal analysis, D.R.K., K.L.D., and W.W.; investigation, C.K.S., D.R.K., and K.L.D.; resources, W.W.; data curation, D.R.K.; writing—original draft preparation, C.K.S. and D.R.K.; writing—review and editing, K.L.D. and W.W.; visualization, K.L.D. and D.R.K.; supervision, K.L.D. and W.W.; project administration, W.W.; funding acquisition, W.W. All authors have read and agreed to the published version of the manuscript.

7.2. Data Availability Statement

The data presented in this study are available on request from the corresponding author.

7.3. Funding and Acknowledgments

This work was supported by the Thammasat University Research Unit in Data Science and Digital Transformation and Thammasat AI Center.

7.4. Conflicts of Interest

The authors declare no conflict of interest.

8. References

[1] Kurotimi, M. F., Franklin, A., Aladei, G., & Helen, O. (2017). Entrepreneurship education as a 21st century strategy for economic growth and sustainable development. International Journal of Mechanical and Industrial Engineering, 11(9), 2242-2253.

[2] Rosenfeld, S. A. (1995). Industrial strength strategies. Aspen Institute, Washington, United States.

[3] Xu, M., David, J. M., & Kim, S. H. (2018). The fourth industrial revolution: Opportunities and challenges. International Journal of Financial Research, 9(2), 90–95. doi:10.5430/ijfr.v9n2p90.

[4] Sharma, P., Gaur, V. K., Gupta, S., Varjani, S., Pandey, A., Gnansounou, E., ... & Wong, J. W. (2022). Trends in mitigation of industrial waste: Global health hazards, environmental implications and waste derived economy for environmental sustainability. Science of the Total Environment, 811, 152357. doi:10.1016/j.scitotenv.2021.152357.

[5] Chowdhary, P., Bharagava, R. N., Mishra, S., & Khan, N. (2020). Role of Industries in Water Scarcity and Its Adverse Effects on Environment and Human Health. Environmental Concerns and Sustainable Development, 1, 235–256. doi:10.1007/978-981-13-5889-0_12.

[6] Lini Dev, K., & Robinson, R. G. (2015). Pond Ash Based Controlled Low Strength Flowable Fills for Geotechnical Engineering Applications. International Journal of Geosynthetics and Ground Engineering, 1(4), 32. doi:10.1007/s40891-015-0035-1.

[7] Bhatt, A., Priyadarshini, S., Acharath Mohanakrishnan, A., Abri, A., Sattler, M., & Techapaphawit, S. (2019). Physical, chemical, and geotechnical properties of coal fly ash: A global review. Case Studies in Construction Materials, 11. doi:10.1016/j.cscm.2019.e00263.

[8] Do, T. M., & Kim, Y. sang. (2016). Engineering properties of controlled low strength material (CLSM) incorporating red mud. International Journal of Geo-Engineering, 7(1), 7. doi:10.1186/s40703-016-0022-y.

[9] Kaliyavaradhan, S. K., Ling, T. C., Guo, M. Z., & Mo, K. H. (2019). Waste resources recycling in controlled low-strength material (CLSM): A critical review on plastic properties. Journal of Environmental Management, 241, 383–396. doi:10.1016/j.jenvman.2019.03.017.

[10] Ibrahim, M., Rahman, M. K., Najamuddin, S. K., Alhelal, Z. S., & Acero, C. E. (2022). A review on utilization of industrial by-products in the production of controlled low strength materials and factors influencing the properties. Construction and Building Materials, 325, 325. doi:10.1016/j.conbuildmat.2022.126704.

[11] Ling, T. C., Kaliyavaradhan, S. K., & Poon, C. S. (2018). Global perspective on application of controlled low-strength material (CLSM) for trench backfilling – An overview. Construction and Building Materials, 158, 535–548. doi:10.1016/j.conbuildmat.2017.10.050.

[12] Le, D. H., & Nguyen, K. H. (2016). An assessment of eco-friendly controlled low-strength material. Procedia Engineering, 142, 260–267. doi:10.1016/j.proeng.2016.02.040.

[13] ACI 229R-99. (1999). Controlled Low-Strength Materials. American Concrete Institute (ACI), Farmington Hills, United States.

[14] Chompoorat, T., Likitlersuang, S., & Jongvivatsakul, P. (2018). The Performance of Controlled Low-strength Material Base Supporting a High-volume Asphalt Pavement. KSCE Journal of Civil Engineering, 22(6), 2055–2063. doi:10.1007/s12205-018-1527-z.

[15] Bassani, M., Khosravifar, S., Goulias, D. G., & Schwartz, C. W. (2015). Long-term resilient and permanent deformation behaviour of controlled low-strength materials for pavement applications. Transportation Geotechnics, 2, 108–118. doi:10.1016/j.trgeo.2014.12.001.

[16] Hoopes, R. (1998). Engineering Properties of Air-Modified Controlled Low-Strength Material. The Design and Application of Controlled Low-Strength Materials (Flowable Fill), 87–101, ASTM International, Pennsylvania, United States. doi:10.1520/stp13064s.

[17] Amlashi, A. T., Abdollahi, S. M., Goodarzi, S., & Ghanizadeh, A. R. (2019). Soft computing based formulations for slump, compressive strength, and elastic modulus of bentonite plastic concrete. Journal of Cleaner Production, 230, 1197–1216. doi:10.1016/j.jclepro.2019.05.168.

[18] Inqiad, W. Bin, Siddique, M. S., Ali, M., & Najeh, T. (2024). Predicting 28-day compressive strength of fibre-reinforced self-compacting concrete (FR-SCC) using MEP and GEP. Scientific Reports, 14(1), 1–21. doi:10.1038/s41598-024-65905-5.

[19] Kumar, S., Kumar, D. R., Wipulanusat, W., & Keawsawasvong, S. (2024). Development of ANN-based metaheuristic models for the study of the durability characteristics of high-volume fly ash self-compacting concrete with silica fume. Journal of Building Engineering, 94, 109844. doi:10.1016/j.jobe.2024.109844.

[20] Zhao, G., Pan, X., Yan, H., Tian, J., Han, Y., & Guan, H. (2024). Predicting engineering properties of controlled low-strength material made from waste soil using optimized SVR models. Case Studies in Construction Materials, 20. doi:10.1016/j.cscm.2024.e03325.

[21] Arachchilage, C. B., Fan, C., Zhao, J., Huang, G., & Liu, W. V. (2023). A machine learning model to predict unconfined compressive strength of alkali-activated slag-based cemented paste backfill. Journal of Rock Mechanics and Geotechnical Engineering, 15(11), 2803–2815. doi:10.1016/j.jrmge.2022.12.009.

[22] Yao, Q., Tu, Y., Yang, J., & Zhao, M. (2024). Hybrid XGB model for predicting unconfined compressive strength of solid waste-cement-stabilized cohesive soil. Construction and Building Materials, 449, 138242. doi:10.1016/j.conbuildmat.2024.138242.

[23] Wang, Y., Chen, G., Xia, J., Yang, H., Zhou, Y., Song, K., & Tan, S. (2025). Experimental and machine learning-based optimization of mix design and compressive strength prediction for a novel dual-waste backfill material. Case Studies in Construction Materials, 23. doi:10.1016/j.cscm.2025.e05152.

[24] Sun, Y. D., Li, C., Bi, Q. Y., Li, J. W., Zhang, J. L., Lu, X. Y., & Yang, Y. (2025). Experimental study and machine learning prediction on compressive strength of industrial waste-solidified marine soft soil under dry-wet cycles. Case Studies in Construction Materials, e04943. doi:10.1016/j.cscm.2025.e04943.

[25] Abdulalim Alabdullah, A., Iqbal, M., Zahid, M., Khan, K., Nasir Amin, M., & Jalal, F. E. (2022). Prediction of rapid chloride penetration resistance of metakaolin based high strength concrete using light GBM and XGBoost models by incorporating SHAP analysis. Construction and Building Materials, 345, 128296. doi:10.1016/j.conbuildmat.2022.128296.

[26] Duan, J., Asteris, P. G., Nguyen, H., Bui, X. N., & Moayedi, H. (2021). A novel artificial intelligence technique to predict compressive strength of recycled aggregate concrete using ICA-XGBoost model. Engineering with Computers, 37(4), 3329–3346. doi:10.1007/s00366-020-01003-0.

[27] Pradeep, T., Samui, P., Kardani, N., & Asteris, P. G. (2022). Ensemble unit and AI techniques for prediction of rock strain. Frontiers of Structural and Civil Engineering, 16(7), 858–870. doi:10.1007/s11709-022-0831-3.

[28] Kumar, R., Kumar, S., Rai, B., & Samui, P. (2024). Development of hybrid gradient boosting models for predicting the compressive strength of high-volume fly ash self-compacting concrete with silica fume. Structures, 66, 66. doi:10.1016/j.istruc.2024.106850.

[29] Jas, K., & Dodagoudar, G. R. (2023). Explainable machine learning model for liquefaction potential assessment of soils using XGBoost-SHAP. Soil Dynamics and Earthquake Engineering, 165. doi:10.1016/j.soildyn.2022.107662.

[30] Kumar, D. R., Samui, P., & Burman, A. (2022). Prediction of Probability of Liquefaction Using Soft Computing Techniques. Journal of The Institution of Engineers (India): Series A, 103(4), 1195–1208. doi:10.1007/s40030-022-00683-9.

[31] Su, J., Wang, Y., Niu, X., Sha, S., & Yu, J. (2022). Prediction of ground surface settlement by shield tunneling using XGBoost and Bayesian Optimization. Engineering Applications of Artificial Intelligence, 114, 105020. doi:10.1016/j.engappai.2022.105020.

[32] Xiao, R., Polaczyk, P., Jiang, X., Zhang, M., Wang, Y., & Huang, B. (2021). Cementless controlled low-strength material (CLSM) based on waste glass powder and hydrated lime: Synthesis, characterization and thermodynamic simulation. Construction and Building Materials, 275. doi:10.1016/j.conbuildmat.2020.122157.

[33] Tran, D. T., Onjaipurn, T., Kumar, D. R., Chim-Oye, W., Keawsawasvong, S., & Jamsawang, P. (2024). An eXtreme Gradient Boosting prediction of uplift capacity factors for 3D rectangular anchors in natural clays. Earth Science Informatics, 17(3), 2027–2041. doi:10.1007/s12145-024-01269-8.

[34] Jalal, F. E., & Iqbal, M. (2023). Unconfined compression strength modelling of expansive soils for sustainable construction: GEP vs MEP. Environmental Earth Sciences, 82(14), 1–12. doi:10.1007/s12665-023-11049-0.

[35] Liu, K., Zhang, L., Wang, W., Zhang, G., Xu, L., Fan, D., & Yu, R. (2023). Development of compressive strength prediction platform for concrete materials based on machine learning techniques. Journal of Building Engineering, 80, 107977. doi:10.1016/j.jobe.2023.107977.

[36] Kardani, N., Bardhan, A., Roy, B., Samui, P., Nazem, M., Armaghani, D. J., & Zhou, A. (2022). A novel improved Harris Hawks optimization algorithm coupled with ELM for predicting permeability of tight carbonates. Engineering with Computers, 38, 4323–4346. doi:10.1007/s00366-021-01466-9.

[37] Sheen, Y. N., Zhang, L. H., & Le, D. H. (2013). Engineering properties of soil-based controlled low-strength materials as slag partially substitutes to Portland cement. Construction and Building Materials, 48, 822-829. doi:10.1016/j.conbuildmat.2013.07.046.

[38] ASTM D4832-16e1. (2023). Standard Test Method for Preparation and Testing of Controlled Low Strength Material (CLSM) Test Cylinders. ASTM International, Pennsylvania, United States. doi:10.1520/D4832-16E01.

[39] ASTM D6103-04. (2013). Standard Test Method for Flow Consistency of Controlled Low Strength Material (CLSM) (Withdrawn 2013). ASTM International, Pennsylvania, United States.

[40] ASTM D6023-07. (2015). Standard Test Method for Density (Unit Weight), Yield, Cement Content, and Air Content (Gravimetric) of Controlled Low-Strength Material (CLSM). ASTM International, Pennsylvania, United States. doi:10.1520/D6023-07.

[41] Bardhan, A., Biswas, R., Kardani, N., Iqbal, M., Samui, P., Singh, M. P., & Asteris, P. G. (2022). A novel integrated approach of augmented grey wolf optimizer and ANN for estimating axial load carrying-capacity of concrete-filled steel tube columns. Construction and Building Materials, 337, 127454. doi:10.1016/j.conbuildmat.2022.127454.

[42] Kumar, S., Rai, B., Biswas, R., Samui, P., & Kim, D. (2020). Prediction of rapid chloride permeability of self-compacting concrete using Multivariate Adaptive Regression Spline and Minimax Probability Machine Regression. Journal of Building Engineering, 32, 101490. doi:10.1016/j.jobe.2020.101490.

[43] Biswas, R., Rai, B., Samui, P., & Roy, S. S. (2020). Estimating concrete compressive strength using MARS, LSSVM and GP. Engineering Journal, 24(2), 41–52. doi:10.4186/ej.2020.24.2.41.

[44] Kumar, S., Kumar, R., Rai, B., & Samui, P. (2024). Prediction of compressive strength of high-volume fly ash self-compacting concrete with silica fume using machine learning techniques. Construction and Building Materials, 438, 136933. doi:10.1016/j.conbuildmat.2024.136933.

[45] Dev, K. L., Kumar, D. R., & Wipulanusat, W. (2024). Machine learning prediction of the unconfined compressive strength of controlled low strength material using fly ash and pond ash. Scientific Reports, 14(1), 27540. doi:10.1038/s41598-024-78050-w.

[46] Nash, J. E., & Sutcliffe, J. V. (1970). River flow forecasting through conceptual models part I - A discussion of principles. Journal of Hydrology, 10(3), 282–290. doi:10.1016/0022-1694(70)90255-6.

[47] Chai, T., & Draxler, R. R. (2014). Root mean square error (RMSE) or mean absolute error (MAE)? -Arguments against avoiding RMSE in the literature. Geoscientific Model Development, 7(3), 1247–1250. doi:10.5194/gmd-7-1247-2014.

[48] Kumar, M., Biswas, R., Kumar, D. R., Pradeep, T., & Samui, P. (2022). Metaheuristic models for the prediction of bearing capacity of pile foundation. Geomechanics and Engineering, 31(2), 129–147. doi:10.12989/gae.2022.31.2.129.

[49] Kumar, D. R., Samui, P., & Burman, A. (2022). Prediction of probability of liquefaction using hybrid ANN with optimization techniques. Arabian Journal of Geosciences, 15(20), 1587. doi:10.1007/s12517-022-10855-3.

[50] Friedman, J. H. (2002). Stochastic gradient boosting. Computational Statistics and Data Analysis, 38(4), 367–378. doi:10.1016/S0167-9473(01)00065-2.

[51] Natekin, A., & Knoll, A. (2013). Gradient boosting machines, a tutorial. Frontiers in Neurorobotics, 7(DEC), 21. doi:10.3389/fnbot.2013.00021.

[52] Freund, Y., & Schapire, R. E. (1996). Experiments with a new boosting algorithm. Proceedings of the Thirteenth International Conference (ICML '96), 3-6 July, 1996, Bari, Italy.

[53] Chen, T., & Guestrin, C. (2016). XGBoost. Proceedings of the 22nd ACM SIGKDD International Conference on Knowledge Discovery and Data Mining, 785–794. doi:10.1145/2939672.2939785.

[54] Xia, Y., Liu, C., Li, Y. Y., & Liu, N. (2017). A boosted decision tree approach using Bayesian hyper-parameter optimization for credit scoring. Expert Systems with Applications, 78, 225–241. doi:10.1016/j.eswa.2017.02.017.

[55] Zhou, J., Qiu, Y., Zhu, S., Armaghani, D. J., Khandelwal, M., & Mohamad, E. T. (2021). Estimation of the TBM advance rate under hard rock conditions using XGBoost and Bayesian optimization. Underground Space (China), 6(5), 506–515. doi:10.1016/j.undsp.2020.05.008.

[56] Breiman, L. (2001). Random Forests. Machine Learning, 45(1), 5–32. doi:10.1023/a:1010933404324.

[57] Belgiu, M., & Drăgu, L. (2016). Random forest in remote sensing: A review of applications and future directions. ISPRS Journal of Photogrammetry and Remote Sensing, 114, 24–31. doi:10.1016/j.isprsjprs.2016.01.011.

[58] Kim, Y. sang, Do, T. M., Kim, M. J., Kim, B. J., & Kim, H. K. (2018). Utilization of by-product in controlled low-strength material for geothermal systems: Engineering performances, environmental impact, and cost analysis. Journal of Cleaner Production, 172, 909–920. doi:10.1016/j.jclepro.2017.10.260.

[59] Dev, K. L., Kumar, D. R., & Wipulanusat, W. (2025). Performance Evaluation of Pond Ash-Enhanced Flowable Fill for Plastic Concrete Cutoff Walls in Earthen Dams Using Advanced Machine Learning Models. Arabian Journal for Science and Engineering, 1–25. doi:10.1007/s13369-025-10228-4.

[60] Jitchaijaroen, W., Ranjan Kumar, D., Keawsawasvong, S., Wipulanusat, W., & Jamsawang, P. (2024). Hybrid artificial neural network models for bearing capacity evaluation of a strip footing on sand based on Bolton failure criterion. Transportation Geotechnics, 48. doi:10.1016/j.trgeo.2024.101347.

[61] Shin, Y., Jang, J. G., Choi, J., Jun, G., Park, C., Kim, G. M., & Yang, B. (2023). Utilization of artificial interior stone sludge as fine aggregate in controlled low-strength material (CLSM). Journal of Building Engineering, 71. doi:10.1016/j.jobe.2023.106441.

[62] Pant, A., & Ramana, G. V. (2022). Prediction of pullout interaction coefficient of geogrids by extreme gradient boosting model. Geotextiles and Geomembranes, 50(6), 1188–1198. doi:10.1016/j.geotexmem.2022.08.003.